Spatial-temporal convergence properties of the Tri-Lab Verification Test suite in 1D for code project A

Francis X. Timmes X-2
Bruce Fryxell X-2
George M. Hrbek X-1

Los Alamos National Laboratory
Los Alamos, NM 87545 USA

September 29, 2006

LA-UR-06-6444

List of Figures

List of Tables

1. Summary

What's New:

- Spatial-temporal verification analysis on uniform and adaptive meshes for the Tri-Lab Verification Test Suite. Previous efforts considered only the quantification of spatial discretization errors at fixed values of the time-step controller (Timmes, Gisler & Hrbek 2005). However, solutions of partial differential equations involve taking discrete time steps. In this report we examine the sensitivity of the simulation results to the magnitude of the time step and possible correlations of the spatial and temporal errors.
- The Tri-Lab Verification Test suite has become part of the daily regression testing. Daily execution of script generates the RAGE input decks, runs the code, compares the numerical and analytical solutions, performs the spatial-temporal verification analysis, and plots the key results (Ankeny & Brock 2006).
- New initialization module for Reinicke Meyer-ter-Vehn problem drastically reduces the size of a RAGE input deck while providing a more accurate and smoother initial state. This is of particular importance for spatial-temporal convergence studies on adaptive meshes.
- LLNL's B-division verification efforts on the Tri-Lab Verification Test Suite is using 4 of our analytic solution codes (Frank Graziani, Carole Woodward).
- Archiving analytic solution codes, input decks, and results on SourceForge. Building on previous efforts often required knowing who to ask for what. All relevant material is now stored in a centralized repository.

Results:

- In general, RAGE shows linear rates of convergence in the temporal domain on the Tri-Lab Test Suite. This is consistent with RAGE's first-order accurate time integration procedure, and comparable to what similar codes (e.g., FLASH or ENZO) produce for some of these test problems. For a few test problems the global error norm does not decrease as the temporal resolution is increased (e.g., Noh, Sedov) because of large persistent errors at discontinuities and boundaries.
- The error budget for each test problem tends to be dominated by either spatial discretization or temporal discretization errors. We found no cases with significant spatial-temporal cross terms. This result may be due to our choice of fixing the time-step control value rather than the time-step Δt itself.

Recommended Directions:

- Continue developing and applying rigorous calculation verification procedures for intricate physics problems that don't admit an exact solution (Smitherman, Kamm & Brock 2005; Tippett & Timmes 2006). This is a key growth direction for verification efforts to bridge the gap between analytical test problems and highly-complex applications.
- Replace the Mader HE detonation test problem. The parameters of Forest-Fire model are cell size and equation

of state dependent, which presents serious difficulties for performing verification studies on different meshes. If the purpose of this test problem in the Tri-Lab Verification Test Suite is to verify detonation wave physics, then there are several detonation problems which have far less idiosyncrasies. If the purpose of the test problem is to verify HE burn models, then additional plans are needed to determine how the model parameters are determined.

- This report on spatial-temporal convergence properties and its companion report on multi-dimensional versions (Timmes, Fryxell & Hrbek 2006) represent a certain closure to research efforts on Tri-Lab Verification Test Suite as it is presently defined (see Figure 1) . New problems that exercise multi-material and/or multi-temperature solutions in an extension of the Tri-Lab Verification Test Suite will be discussed with Livermore and Sandia at the 2006 Nuclear Explosives Code Developers Conference.

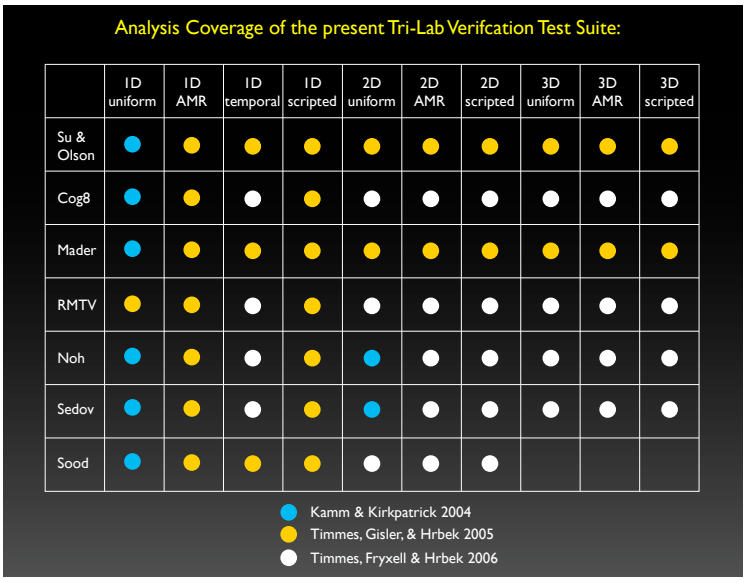

Figure 1. - Status of LANL's efforts on the Tri-Lab Verification Test Suite. Pioneering efforts by Kamm & Kirkpatrick (2004) supplied verification analyses on most of the problems on 1D uniform grids and for two problems on 2D uniform grids. Timmes, Gisler & Hrbek (2005) automated the verification process, extended coverage to adaptive meshes, initiated temporal domain verification, and ran additional problems in 2D and 3D. The present effort establishes spatial-temporal convergence and multi-dimensional versions of all the problems on uniform and adaptive meshes.

2. Tri-Lab Verification Test Suite

Numerical solution methods for partial-differential equations discretize continuum fields in space and time. This finite approximation of continuum fields embeds discretization errors into numerical simulations that are modeled by a postulated error equation (Brock 2004). Verification analysis, the study of the error model, should encompass both space and time convergence studies. These analyses should be conducted in the time and space asymptotic regimes where the numerical error is uniformly reduced as the discretization parameters are refined. The extent of each asymptotic regime and any relationship between these regimes, however, are not well defined prior to conducting the numerical simulations. Previous efforts considered only the quantification of spatial discretization errors in the solutions to the Tri-Lab Verification Test Suite (Timmes, Gisler & Hrbek 2005). This report focuses on the spatial and temporal convergence properties of the Tri-Lab Test Suite in 1D using programs from Code Project A.

The Tri-Lab verification test suite is presently defined by seven problems that have analytical solutions: Su & Olson, Mader, Reinicke Meyer-ter-Vehn, Coggeshall #8, Noh, Sedov, and Sood (Kamm & Kirkpatrick 2004; Figure 1). In this report, RAGE 20060331.0240 was run on the Linux cluster Flash to generate numerical solutions on 1D uniform grids for all the Tri-Lab problems (NOBEL 20050331.021 was used for the Mader problem). The RAGE input decks used are the same ones archived by Timmes, Gisler & Hrbek (2005), although several of the input decks were modified to accommodate improvements made to the RAGE test modules (Clover 2006) or to generalize their contents to include temporal or multi-dimensional capability. These updated decks are shown in Appendix A.

After the problems were run, John Grove's AMHCTOOLS (2005a, 2005b) was used to extract the solution data on the native grid from the binary dump files. If one requests the simulation data from RAGE, the data on the native mesh is interpolated onto uniform mesh. Extracting the solution data on the native mesh is important for proper verification analysis, particularly on adaptive meshes.

After the numerical solution on the native grid was extracted, the absolute L_1 norm and absolute L_2 norm were computed (Kamm, Rider, Brock 2002) as

$$L_{1,\mathrm{abs}} = \frac{\sum (f_i^{\mathrm{exact}} - f_i^{\mathrm{rage}}) V_i}{\sum V_i} \qquad L_{2,\mathrm{abs}} = \left[\frac{\sum (f_i^{\mathrm{exact}} - f_i^{\mathrm{rage}})^2 V_i}{\sum V_i} \right]^{1/2} \tag{1}$$

where V_i is the appropriate volume element weighting, and f denotes a state variable such as pressure or density. To be specific, one-dimensional versions of the Su-Olson, Mader, and Sood problems run in slab geometry have $V_i = \Delta x_i$ where Δx_i is the grid spacing. Spherically symmetric Reinicke Meyer-ter-Vehn, Coggeshall #8, Noh, and Sedov problems use the shell volume $V_i = 4/3\pi(r^3_{\mathrm{outer}} - r^3_{\mathrm{inner}})$. In this manner the norm weights correspond to how the variable of interest is treated in the solver, e.g., volume averaged variables have volume norm weights.

After the global error norms were computed, the rates of convergence were determined. For cases where the time-step controller was held constant and the spatial resolution varied, the $L_{1,\mathrm{abs}}$ error norm was assumed to obey

$$L_{1,\mathrm{abs}} = A\,(\Delta x)^{\alpha} \quad , \tag{2}$$

where Δx is the cell spacing and α is the spatial convergence rate (Kamm, Rider, & Brock 2002). In this case the rate of convergence between two grids, one coarse and one fine, is given explicitly by

$$\alpha = \log\left[\frac{L_{1,\mathrm{abs,fine}}}{L_{1,\mathrm{abs,coarse}}}\right] \Big/ \log\left[\frac{\Delta x_{\mathrm{fine}}}{\Delta x_{\mathrm{coarse}}}\right] \quad . \tag{3}$$

This error model follows from a modified-equation analysis which is typically done in terms of length scales - not volumes. That is, while some problems may use volume elements to compute an error norm, the error model always uses grid spacings. This raises a pragmatic issue, particularly for problems run with adaptive mesh refinement. The RAGE dump files, which are cracked by AMHCTOOLS, reports the cell's volume. For 1D Cartesian coordinates the volume reported is the mesh spacing Δx, which is suitable for the error norm and convergence calculations. For 1D spherical coordinates the volume reported is the shell volume, which is suitable for the error norm calculation, but we need Δr for the convergence calculations. While RAGE/AMHCTOOLS reports the cell center r, it doesn't directly report either the mesh spacing Δr or the inner and outer radii of the spherical shell. We derived the radial mesh spacing as follows. The volume of a spherical shell is

$$V = \frac{4\pi}{3}\left(r_{\text{outer}}^3 - r_{\text{inner}}^3\right) = \frac{4\pi}{3}\left[\left(r + \frac{\Delta r}{2}\right)^3 - \left(r - \frac{\Delta r}{2}\right)^3\right] \quad . \tag{4}$$

With the shell volume V and cell center r known, solving for Δr yields

$$(\Delta r)^3 + 12r^2\Delta r - \frac{3V}{\pi} = 0 \quad . \tag{5}$$

There is only one real root to this cubic, given by $\Delta r = u + v$, where

$$u = \left(p + \sqrt{q}\right)^{1/3} \qquad v = -\frac{c}{3u}$$

$$p = -\frac{d}{2} \qquad q = p^2 + \left(\frac{c}{3}\right)^3$$

$$c = 12r^2 \qquad d = -\frac{3V}{\pi} \quad , \tag{6}$$

For spherical symmetry in 2D r-z coordinates, the shell volume is

$$V = \pi\Delta h\left(r_{\text{outer}}^2 - r_{\text{inner}}^2\right) = \pi\Delta h\left[\left(r + \frac{\Delta r}{2}\right)^2 - \left(r - \frac{\Delta r}{2}\right)^2\right] \quad . \tag{7}$$

Since RAGE enforces square cells, $\Delta h = \Delta r$, and the solution for the radial grid spacing reduces to a simple quadratic whose solution is

$$\Delta r = \sqrt{\frac{V}{2\pi r}} \tag{8}$$

Equations (7) and (8) are valid on both uniform and adaptive meshes in RAGE.

For cases where the spatial resolution was held constant and the temporal resolution varied, the global error norms were assumed to obey

$$L_{1,\text{abs}} = B\left(\Delta t\right)^{\beta} \tag{9}$$

where Δt is the time-step and β is the temporal convergence rate. In this case the rate of convergence between two temporal resolutions, one coarse and one fine, is given explicitly by

$$\beta = \log\left[\frac{L_{1,\text{abs,fine}}}{L_{1,\text{abs,coarse}}}\right] \Big/ \log\left[\frac{\Delta t_{\text{fine}}}{\Delta t_{\text{coarse}}}\right] \quad . \tag{10}$$

When both the time-step controller and spatial resolution were varied, the global error norms were assumed to obey

$$L_{1,\mathrm{abs}} = A\,(\Delta x)^{\alpha} + B\,(\Delta t)^{\beta} + C\,(\Delta x \Delta t)^{\gamma} \quad . \tag{11}$$

The $\Delta x \Delta t$ term expresses, to first order, a potential interplay between the space and time resolutions. Other forms of the interaction between space and time, such as $\Delta x/\Delta t$ or $(\Delta x)^2/\Delta t$ or $(\Delta x)^{\gamma_1}(\Delta t)^{\gamma_2}$, were not investigated in this report.

The coefficients and powers in this equation were determined from minimizing the chi-square fit between the data (the L_1 error norms) and the model (equation 11). For this task we used the Marquardt-Levenberg algorithm implemented in gnuplot 4.0 (Williams et al. 2004). Gnuplot is a command-line driven interactive function plotting utility for many types of operating systems and platforms. An advantage of using gnuplot is that the determination of the six coefficients in equation (6) can be easily incorporated into an automated work-flow. A potential disadvantage of using a non-linear least squares fitting procedure is that the convergence parameters derived may not be unique.

How should the time step be chosen? It could be held fixed, at a value suitable for the finest grid considered, and the spatial resolution varied. A ratio of the time-step to the cell size could be held constant. For example, $\Delta x/\Delta t$ could be held fixed (ala a Courant number) which would be suitable for purely hydrodynamic problems, or the ratio $(\Delta x)^2/\Delta t$ could held fixed for diffusion dominated problems. For this report, we considered fixed values of a time-step controller (e.g., RAGE's cstab, de_tecpct, or tstab). This approach has the advantage of being easy to apply and interpret in practical simulations, but has the disadvantage of having time-steps that are not precisely constant. Thus, for this report, we will fit an error ansatz of the form

$$L_{1,\mathrm{abs}} = A\left(\frac{\mathrm{ngrid\_norm}}{\mathrm{ngrid}}\right)^{\alpha} + B\left(\frac{\mathrm{tcontrol}}{\mathrm{tcontrol\_norm}}\right)^{\beta} + C\left(\frac{\mathrm{ngrid\_norm}\cdot\mathrm{tcontrol}}{\mathrm{ngrid}\cdot\mathrm{tcontrol\_norm}}\right)^{\gamma} \quad , \tag{12}$$

where ngrid is the number of grid points, ngrid_norm a normalization value for the number of grid points, tcontrol is the value of the parameter controlling the time step, and tcontrol_norm a normalization value of the parameter controlling the time step. The purpose of the normalizations is to allow the pre-factors A, B, C to have the same units as the $L_{1,\mathrm{abs}}$ error norm.

It should be noted that the spatial discretization errors, temporal discretization errors, or coupled space-time errors may change with time during the numerical simulation. As various physical effects are exercised in different proportions during an evolution, the dominant contributor to the overall numerical error may not remain the same (Hemez 2005). For example, the effects of time discretization on a hydrodynamic simulation may be more pronounced early in the evolution. Likewise, inadequate spatial discretization at some instants of the simulation may be replaced as the dominant source of solution error by truncation errors at other times (Hemez 2005). These remarks imply that convergence coefficients in equations 2, 9 or 11 may be functions of spacetime. To keep the present study practical, we consider only the code verification properties at the ending time of a test problem's evolution.

The foregoing analysis has become part of the daily regression testing. That is, daily execution of script that generates the RAGE input decks, runs the code, compares the numerical and analytical solutions, performs the spatial-temporal verification analysis, and plots the key results (Hrbek et al., 2005; Ankeny & Brock 2006).

The remainder of this report details the verification analysis of the Tri-Lab Verification Test Suite, focusing on the temporal convergence rates and the interplay (if any) with the spatial resolution of the simulation.

2.1 The Su & Olson Problem

The Su & Olson problem is a one-dimensional, half-space, non-equilibrium Marshak wave problem. There is no hydrodynamics in this test problem. The radiative transfer model is a one-group diffusion approximation with a finite radiation source boundary condition, where the radiative and material fields are out of equilibrium. As the energy density of the radiation field increases, energy is transfered to the material (see Figure 2). Su & Olson (1996) found a quadrature solution for the distribution of radiative energy and material temperature as a function of spacetime. This problem is useful for verifying time-dependent radiation diffusion codes. A succinct description of the Su & Olson problem for the Tri-Lab Verification Test Suite along with fortran code for generating solutions are discussed in Timmes, Gisler & Hrbek (2005).

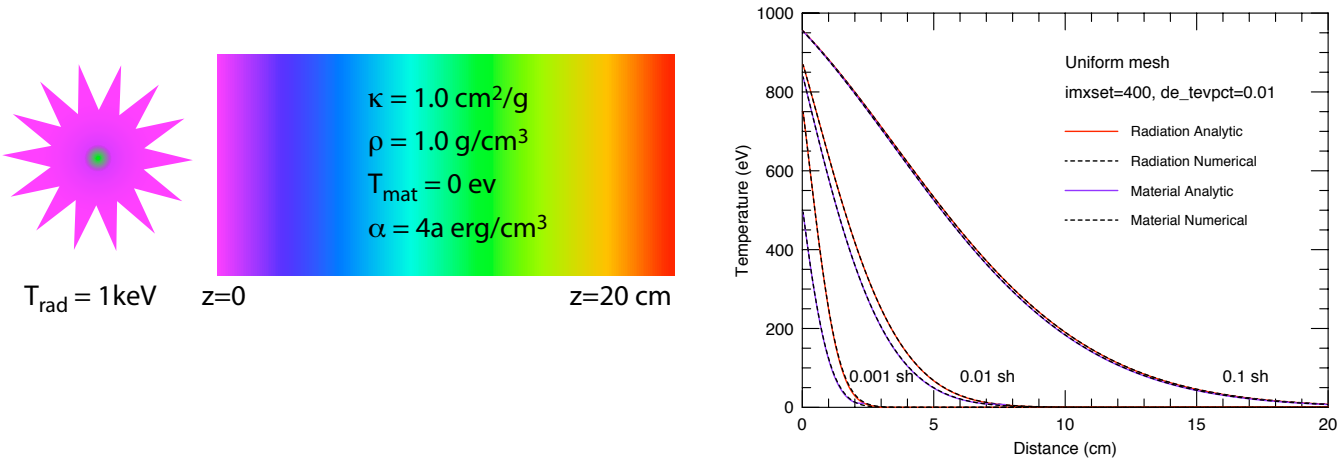

Figure 2. - Setup and parameters for the Su & Olson problem are illustrated on the left. On the right are numerical (black dotted curves) and analytical solutions for the radiation temperature (solid purple curves) and material temperature (solid red curves) on a uniform grid of 400 cells and a time-step controller of de_tevpct=0.01.

Figure 2 shows a representative solution on a uniform mesh of 400 cells. The parameter de_tevpct sets the maximum relative radiation temperature change allowed per time-step, and is used to determine the time-step in the numerical solution of the Su & Olson problem. It was set at a relatively strict value of 0.01, limiting changes in the radiation temperature to a maximum of 1% in a time-step. Solutions are shown at 0.001, 0.01 and 0.1 sh. Initially, the radiation streams into the slab and the material temperature lags behind the radiation temperature. As the radiation energy density builds up, the material temperature catches up, and by t = 0.1 sh, the radiation and material temperatures are essentially identical.

Figure 3 shows the absolute value of the relative errors in the radiation temperature and material temperature for one-dimensional uniform grids with 100, 200, 400, 800, 1600, and 3200 cells at the final time of 0.1 shake. The time-step controller was set to de_tevpct=0.01. The cusps are due to changes of sign in the relative error, and the relative cpu cost on a single processor of increasing the spatial resolution is shown. Figure 3 suggests, and Table 1 demonstrates, that the radiation and material temperatures are in the asymptotic regime with roughly linear convergence rates at this

time-step control setting.

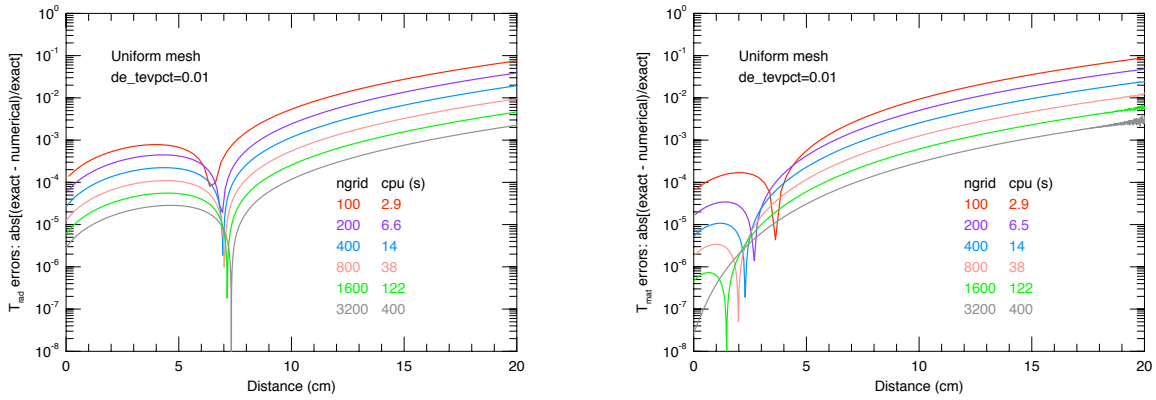

Figure 3. - Absolute value of the relative error in the radiation temperature (left) and material temperature (right) fields for a variety of uniform grids at a fixed time-step control value of de_tevpct=0.01.

Table 1
Spatial Convergence Coefficients for the Su & Olson Problem

	T_{rad}			T_{mat}		
# of cells	$L_{1,abs}$	α	A	$L_{1,abs}$	α	A
100	6.781E-01			8.715E-01		
200	3.364E-01	1.011E+00	2.755E+00	4.778E-01	8.671E-01	2.899E+00
400	1.666E-01	1.014E+00	2.768E+00	2.452E-01	9.625E-01	3.535E+00
800	8.204E-02	1.022E+00	2.834E+00	1.241E-01	9.824E-01	3.736E+00
1600	4.106E-02	9.987E-01	2.614E+00	6.430E-02	9.485E-01	3.322E+00
3200	2.119E-02	9.539E-01	2.169E+00	3.466E-02	8.917E-01	2.623E+00

Figure 4 shows absolute value of the relative errors in the radiation temperature and material temperatures for de_tevpct=0.4, 0.2 (the default value), 0.1, 0.05, 0.02, 0.01, 0.0002, 0.001 on one-dimensional uniform grids with 100 and 1600 cells at the final time of 0.1 shake. The near constant cpu time for the largest values are due to another time-step constraint; the growth of the initial time step from a very small value. Figure 4 suggests the radiation temperature has a convergence rate of $\beta \sim 1$ while the material temperature has $\beta \sim 0.8$ at the highest spatial resolutions considered. Table 2 details the convergence properties and shows that the aforementioned convergence rates degrade at lower spatial resolutions.

Figure 5 shows the $L_{1,abs}$ norms and the residuals of fitting equation (12) to the $L_{1,abs}$ norms of the radiation and material temperatures when the time-step controller and spatial resolution are varied. The plus signs indicate the spatial and temporal points (the data points) where the $L_{1,abs}$ norm was computed. The images on the left show the $L_{1,abs}$ norm (the data) while the images on the right show the relative residual of fitting the $L_{1,abs}$ norm to the error model (equation 12). If the residuals of the non-linear least squares fitting procedure are small, then the derived convergence rates are probably reliable. Table 3 details the derived spacetime convergence rates. The spacetime

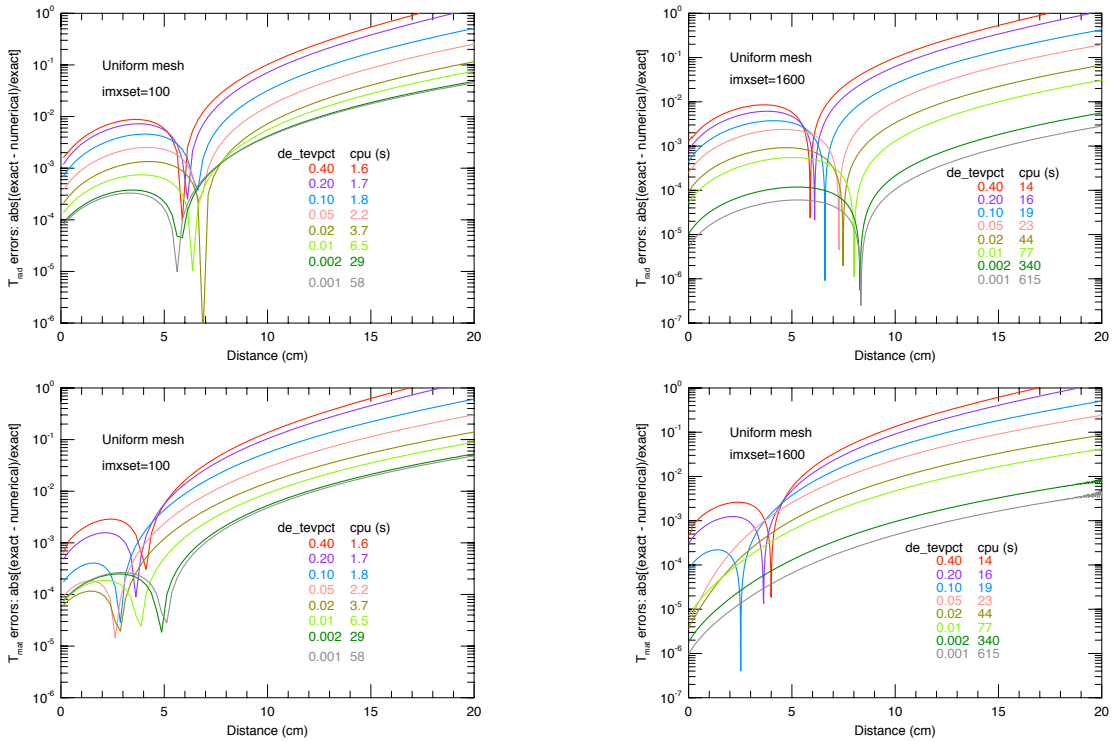

Figure 4. - Absolute value of the relative error in the radiation temperature (upper) and material temperature (lower) fields for a variety of de_tevpct time-step control values on uniform grids of 100 and 1600 cells.

Table 2
Temporal Convergence Coefficients for the Su & Olson Problem

		T_{rad}			T_{mat}		
ngrid	de_tevpct	$L_{1,abs}$	β	B	$L_{1,abs}$	β	B
100	0.4	1.346E+01			1.501E+01		
	0.2	9.332E+00	5.280E-01	2.183E+01	1.090E+01	4.620E-01	2.292E+01
	0.1	4.188E+00	1.156E+00	5.999E+01	5.420E+00	1.008E+00	5.518E+01
	0.05	2.101E+00	9.954E-01	4.143E+01	2.806E+00	9.495E-01	4.824E+01
	0.02	9.947E-01	8.158E-01	2.419E+01	1.389E+00	7.679E-01	2.800E+01
	0.01	6.787E-01	5.516E-01	8.607E+00	8.831E-01	6.530E-01	1.786E+01
	0.005	5.357E-01	3.414E-01	3.270E+00	6.693E-01	4.001E-01	5.573E+00
	0.002	4.607E-01	1.645E-01	1.280E+00	5.384E-01	2.374E-01	2.354E+00
	0.001	4.376E-01	7.434E-02	7.313E-01	4.965E-01	1.170E-01	1.114E+00
1600	0.4	1.320E+01			1.477E+01		
	0.2	8.256E+00	6.768E-01	2.454E+01	9.659E+00	6.128E-01	2.590E+01
	0.1	3.429E+00	1.268E+00	6.350E+01	4.524E+00	1.094E+00	5.620E+01
	0.05	1.575E+00	1.122E+00	4.543E+01	2.349E+00	9.459E-01	3.994E+01
	0.02	5.514E-01	1.146E+00	4.875E+01	9.027E-01	1.044E+00	5.352E+01
	0.01	2.592E-01	1.089E+00	3.905E+01	4.949E-01	8.670E-01	2.682E+01
	0.005	1.249E-01	1.054E+00	3.317E+01	2.733E-01	8.568E-01	2.560E+01
	0.002	4.962E-02	1.007E+00	2.595E+01	1.411E-01	7.218E-01	1.252E+01
	0.001	2.562E-02	9.536E-01	1.859E+01	9.725E-02	5.364E-01	3.954E+00

convergence rates are generally consistent with values derived when the space and time analyses were performed independently since the $\Delta x \Delta t$ cross-terms have relatively small coefficients and exponents in this regime. This result may be due to our choice of fixing the time-step control value de_tevpct rather than the time-step Δt itself.

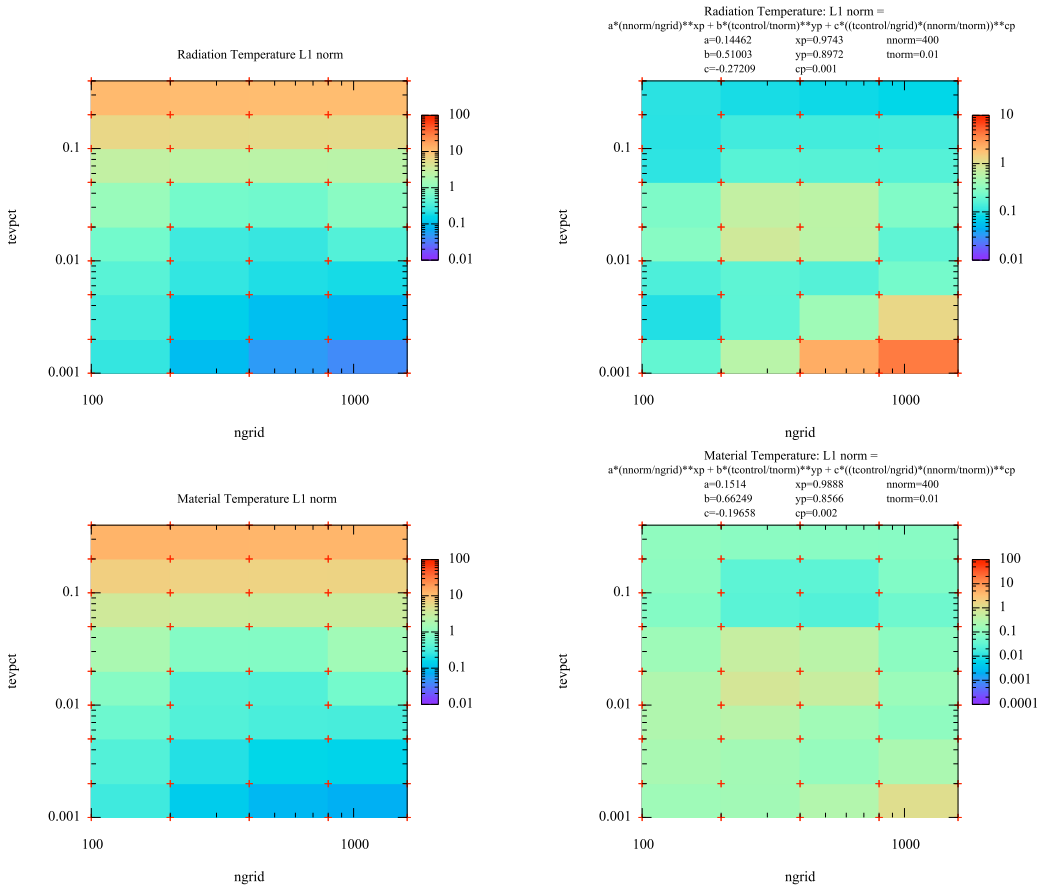

Figure 5. - $L_{1,abs}$ error norms (left) and relative residuals (right) from fitting the error model for the radiation and material temperatures when spatial and temporal resolution are varied. Plus signs indicate the spacetime points where the error norm was computed.

Table 3
Spacetime Convergence Rates for the Su & Olson Problem

Parameter	Radiation Temperature	Material Temperature
A	0.151404	0.144618
α	0.9888	0.9743
ngrid_norm	400	400
B	0.662494	0.510033
β	0.8566	0.8972
tevpct_norm	0.01	0.01
C	-0.196583	-0.272089
γ	0.002	0.001

2.2 The Coggeshall #8 Problem

Coggeshall (1991) published a collection of analytic self-similar test problems, and ``Coggeshall #8" or ``Cog8" is the eighth one listed. The solution to this problem represents an adiabatic expansion plus heat conduction (see Figure 6). The heat conduction's area weighted flux on each cell face is equal. That is, conduction moves as much energy into a cell as it removes. Thus, the answers with and without conduction look much the same (Clover 2006). A succinct description of the Coggeshall problem for the Tri-Lab Verification Test Suite along with fortran code for generating solutions are discussed in Timmes, Gisler & Hrbek (2005).

A new analytic solution for the two-dimensional cell-averaged solution of Cog8 is given by Timmes & Clover (2006). Their comparison of the point-wise solution and cell-averaged solution on a series of uniform grids suggests the cell-averaged field is smoother overall than the point-wise solution. Both point-wise and cell-averaged approaches show similar global $L_{1,abs}$ norms and first-order convergence rates. Their improved two-dimensional cell-averaged solution has been implemented in RAGE's test problem modules.

Figure 6 shows a representative solution on a 1D uniform mesh of 200 cells. The parameter tstab sets the time step allowed by the material speed, $\Delta t = \text{tstab} \cdot \Delta x \,/\, (|v_x| + |v_y| + |v_z|)$, and determines the time-step in the numerical solution of the Cog8 problem. It was set to its default value of 0.2, limiting transport of material to 20% of a cell's width. Solutions are shown for the density, pressure, temperature, and material speed at a time of 20 shakes.

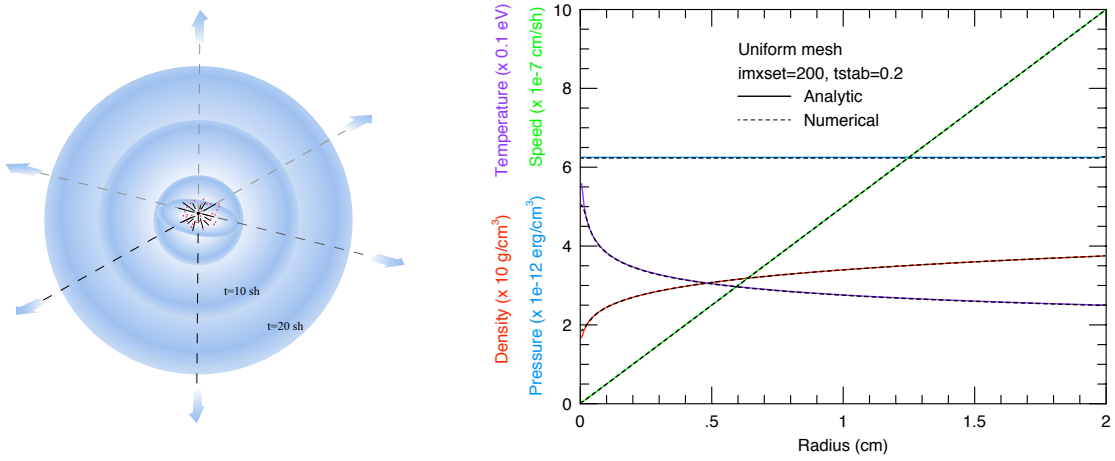

Figure 6. - Setup for the spherically symmetric Coggeshall #8 problem is illustrated on the left. The analytic solution at t=10 sh is used as the initial condition in RAGE, which is then evolved to t=20 sh. On the right are analytical (solid curves) and numerical (dotted curves) solutions at t=20 sh for the mass density (red), velocity (green), pressure (blue), and temperature (purple). The calculation is for a uniform mesh of 200 cells in 1D spherically symmetric geometry and a time-step controller of tstab=0.2.

Figure 7 shows the absolute value of the relative errors in the cell-averaged density, pressure, temperature, and material speed for one-dimensional uniform grids with 100, 200, 400, 800, 1600, and 3200 cells at the final time of 20 sh. The time-step controller was set at its default value, tstab=0.2. Cusps are due to changes of sign in the

relative error, and the relative cpu cost on a single processor of increasing the spatial resolution is shown. In general, the errors get smaller with increasing uniform grid resolution. However, there are large, persistent errors at the boundaries. Getting the right amount of energy to flow into an origin of a sphere is an unsolved problem, so an error accumulates at the origin whether using the point-wise or cell-averaged quantities. Errors at the right boundary are due to the freeze-region boundary conditions. Figure 7 suggests, and Table 4 details, that the pressure and temperature have linear convergence rates while the density and material speed have nearly quadratic convergence rate with spatial resolution at this time-step control setting.

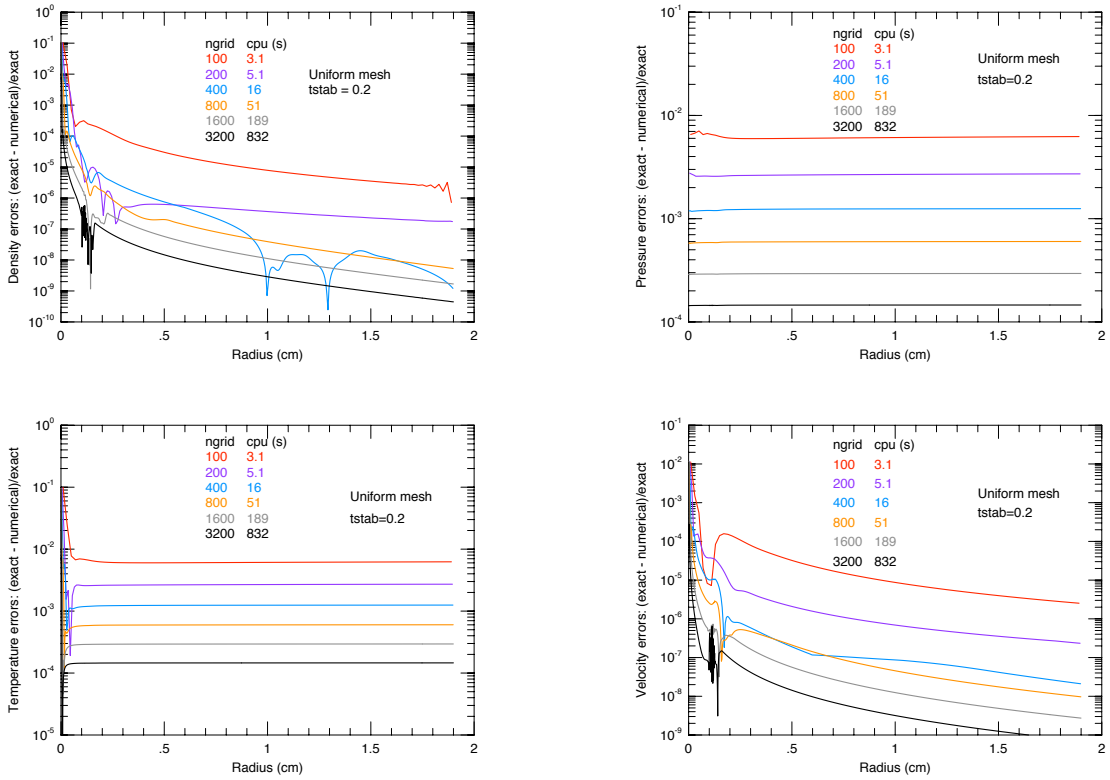

Figure 7. - Absolute value of the relative error in the density (upper left), pressure (upper right), temperature (lower left) and material speed (lower right) for a variety of uniform grids at a fixed time-step control value of tstab=0.2.

Figure 8 shows the absolute value of the relative errors in the density, pressure and radial velocity for tstab=0.8, 0.4, 0.2 (the default value), 0.1, 0.05, and 0.025, on one-dimensional uniform grids of 200 and 1600 cells. Values of tstab $\geq$ 0.4 begin to produce very inaccurate results near the right boundary at the beginning of the simulation, and that error propagates inwards into the domain. For large values of tstab, the Cog #8 test problem violates the recommended accuracy criterion of the code. Neglecting the large values of the time-step controller, Figure 8 suggests and Table 5 shows that at 1600 cells and the smallest values of tstab that the density has a convergence rate $\beta \sim 0$ at 1600 cells, the pressure about $\beta \sim 1$, the temperature about $\beta \sim 0.2$, and the radial velocity about $\beta \sim 0.8$. Table 5 details the convergence properties at other spatial resolutions and time-step controllers.

Table 4
Spatial Convergence Coefficients for the Coggeshall #8 Problem

	Density			Pressure		
# of cells	$L_{1,abs}$	α	A	$L_{1,abs}$	α	A
100	2.044E-06			3.859E+10		
200	1.162E-07	4.137E+00	2.187E+01	1.687E+10	1.193E+00	4.112E+12
400	2.567E-08	2.178E+00	2.637E-03	7.797E+09	1.114E+00	2.849E+12
800	1.093E-08	1.232E+00	1.757E-05	3.752E+09	1.055E+00	2.090E+12
1600	3.061E-09	1.836E+00	6.536E-04	1.840E+09	1.028E+00	1.770E+12
3200	7.913E-10	1.952E+00	1.418E-03	9.114E+08	1.014E+00	1.615E+12
	Temperature			Speed		
# of cells	$L_{1,abs}$	α	A	$L_{1,abs}$	α	A
100	1.634E-01			3.428E+02		
200	7.137E-02	1.195E+00	1.749E+01	2.893E+01	3.567E+00	3.935E+08
400	3.298E-02	1.114E+00	1.205E+01	3.258E+00	3.151E+00	5.788E+07
800	1.587E-02	1.055E+00	8.838E+00	1.641E+00	9.898E-01	6.174E+02
1600	7.786E-03	1.027E+00	7.483E+00	4.582E-01	1.840E+00	1.007E+05
3200	3.856E-03	1.014E+00	6.832E+00	1.174E-01	1.965E+00	2.319E+05

Table 5
Temporal Convergence Coefficients for the Coggeshall #8 Problem

		Density			Pressure		
ngrid	tstab	$L_{1,abs}$	β	B	$L_{1,abs}$	β	B
200	8.000E-01	2.790E-01			1.584E+13		
	4.000E-01	1.569E-02	4.153E+00	7.049E-01	5.376E+11	4.881E+00	4.708E+13
	2.000E-01	1.215E-04	7.013E+00	9.686E+00	1.671E+10	5.008E+00	5.288E+13
	1.000E-01	1.180E-04	4.180E-02	1.300E-04	9.493E+09	8.160E-01	6.214E+10
	5.000E-02	1.169E-04	1.376E-02	1.218E-04	5.871E+09	6.933E-01	4.685E+10
	2.500E-02	1.162E-04	8.664E-03	1.200E-04	4.035E+09	5.409E-01	2.968E+10
1600	8.000E-01	2.815E-01			1.815E+13		
	4.000E-01	1.594E-02	4.143E+00	7.095E-01	5.359E+11	5.082E+00	5.640E+13
	2.000E-01	1.237E-05	1.033E+01	2.061E+02	1.833E+09	8.192E+00	9.751E+14
	1.000E-01	1.202E-05	4.046E-02	1.320E-05	9.303E+08	9.781E-01	8.846E+09
	5.000E-02	1.192E-05	1.217E-02	1.237E-05	4.808E+08	9.524E-01	8.336E+09
	2.500E-02	1.186E-05	7.643E-03	1.220E-05	2.555E+08	9.118E-01	7.383E+09
		Temperature			Speed		
ngrid	tstab	$L_{1,abs}$	β	B	$L_{1,abs}$	β	B
200	8.000E-01	1.498E+01			6.777E+06		
	4.000E-01	9.352E-01	4.001E+00	3.658E+01	2.340E+05	4.856E+00	2.003E+07
	2.000E-01	1.065E-01	3.134E+00	1.652E+01	5.542E+02	8.722E+00	6.918E+08
	1.000E-01	7.460E-02	5.137E-01	2.435E-01	2.659E+02	1.060E+00	3.051E+03
	5.000E-02	5.859E-02	3.485E-01	1.664E-01	1.710E+02	6.368E-01	1.152E+03
	2.500E-02	5.060E-02	2.116E-01	1.104E-01	1.149E+02	5.732E-01	9.521E+02
1600	8.000E-01	1.709E+01			6.707E+06		
	4.000E-01	8.526E-01	4.325E+00	4.486E+01	2.387E+05	4.812E+00	1.963E+07
	2.000E-01	1.417E-02	5.911E+00	1.918E+02	4.860E+01	1.226E+01	1.808E+10
	1.000E-01	1.005E-02	4.962E-01	3.150E-02	1.985E+01	1.292E+00	3.888E+02
	5.000E-02	8.018E-03	3.257E-01	2.127E-02	1.153E+01	7.837E-01	1.206E+02
	2.500E-02	7.014E-03	1.929E-01	1.429E-02	6.589E+00	8.075E-01	1.295E+02

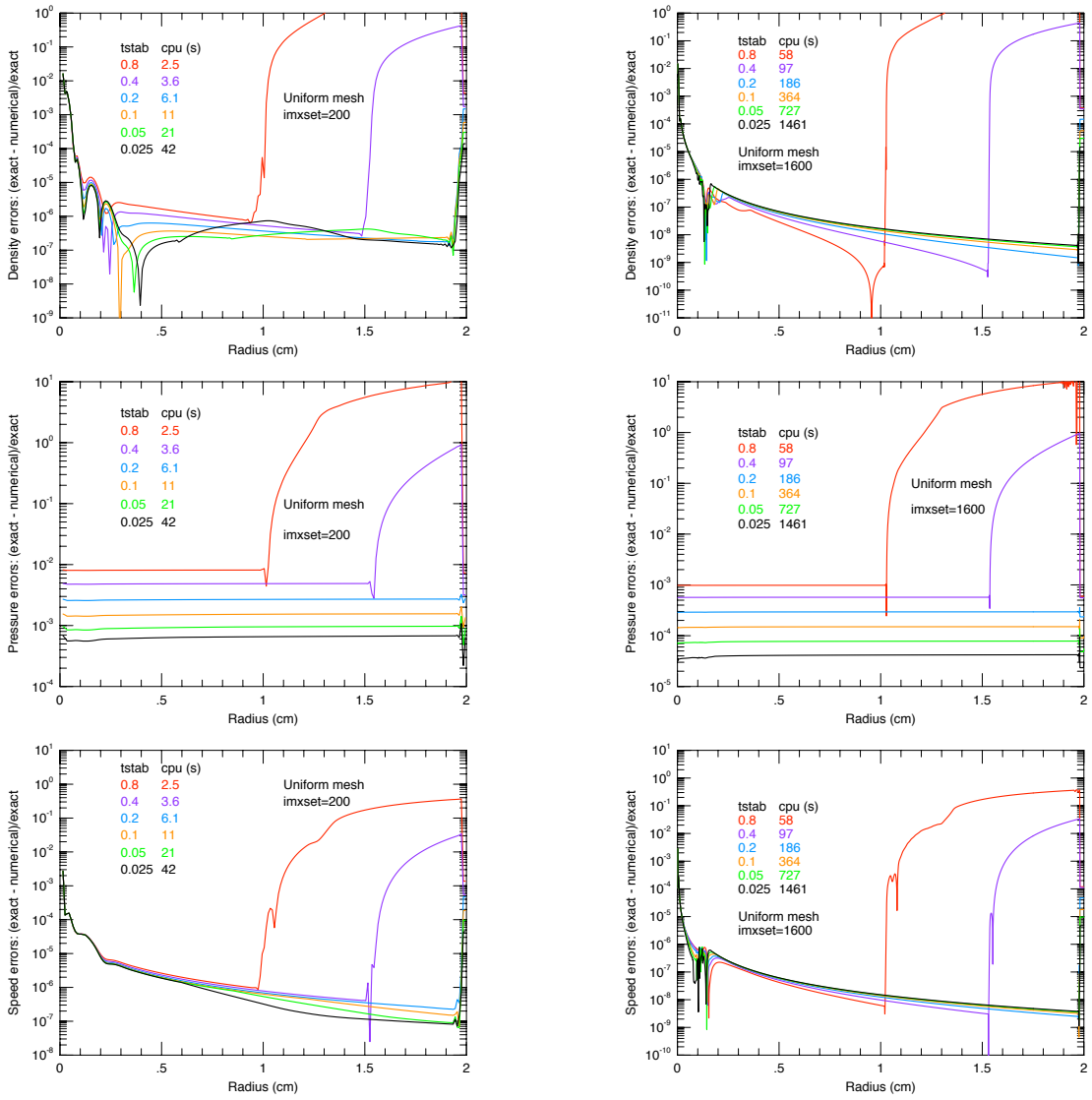

Figure 8. - Absolute value of the relative error in the density (upper), pressure (middle) and material speed (lower) for a variety of tstab time-step control values on uniform grids of 200 and 1600 cells.

Figure 9 shows the $L_{1,abs}$ norms and the residuals of fitting equation (12) to the $L_{1,abs}$ norms of the density, temperature, pressure, and material speed when the time-step controller and spatial resolution are varied. The plus signs indicate the spatial and temporal points (the data points) where the $L_{1,abs}$ norm was computed. The images on the left show the $L_{1,abs}$ norm (the data) while the images on the right show the relative residual of fitting the $L_{1,abs}$ norm to the error model (equation 12). If the residuals of the non-linear least squares fitting procedure are small, then the derived convergence rates are probably reliable. Table 6 details the derived spacetime convergence rates. The fitted rates are generally consistent with values derived when the space and time analyses were performed independently. This may be due to our choice of fixing the time-step control value rather than the time-step Δt itself.

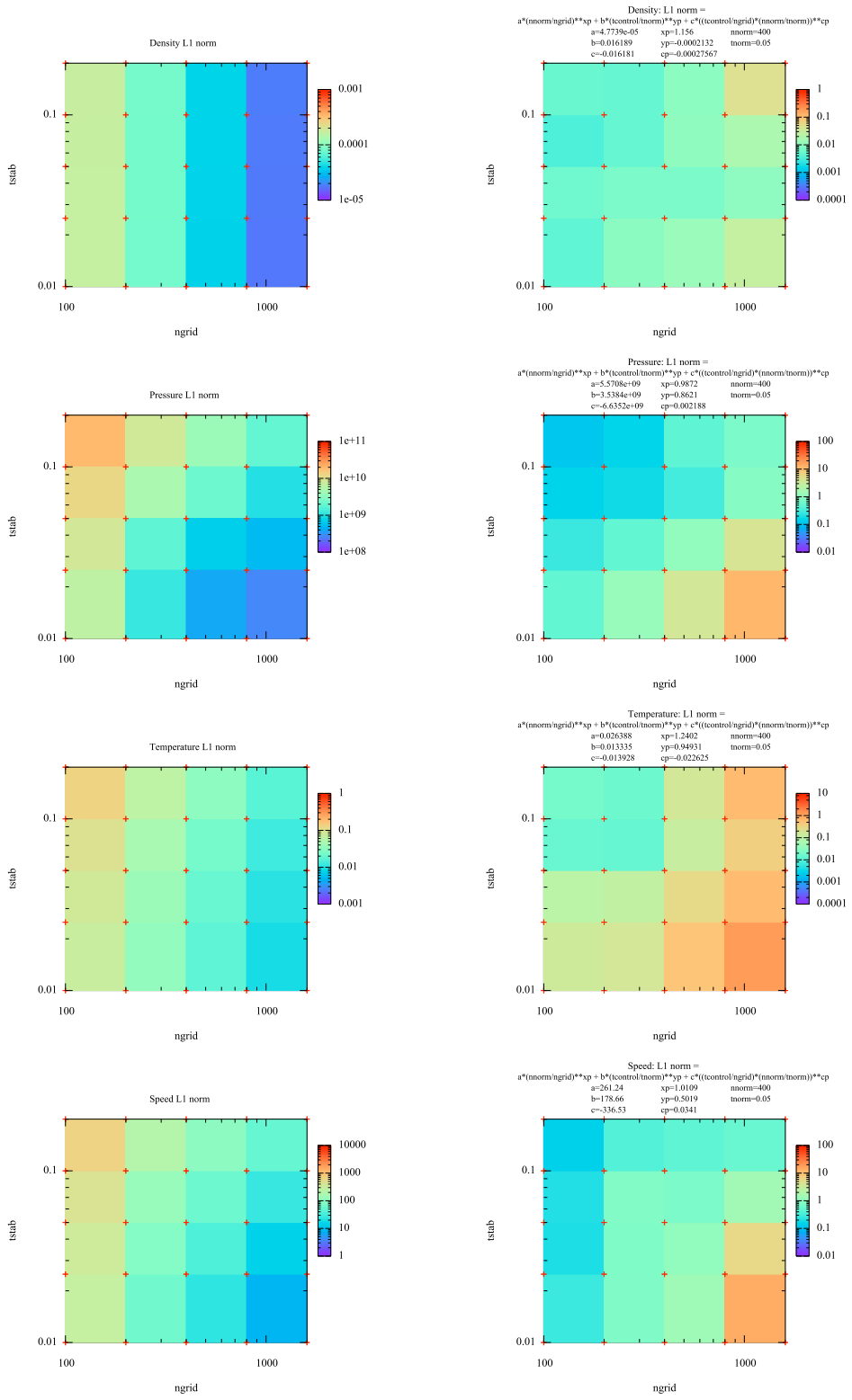

Figure 9. - $L_{1,abs}$ error norms (left) and relative residuals (right) from fitting the error model for the density, temperature, pressure, and material speed when spatial and temporal resolution are varied. Plus signs indicate the spacetime points where the error norm was computed.

Table 6
Spacetime Convergence Rates for the Coggeshall #8 Problem

Parameter	Density	Pressure	Temperature	Material Speed
A	4.77388e-05	5.57082e+09	0.0263884	261.241
α	1.15596	0.9872	1.24016	1.0109
ngrid_norm	400	400	400	400
B	0.0161895	3.5384e+09	0.0133355	178.664
β	-0.0002132	0.8621	0.94931	0.5019
tstab_norm	0.05	0.05	0.05	0.05
C	-0.016181	-6.63519e+09	-0.0139284	-336.529
γ	-0.000275672	0.002188	-0.0226245	0.0341

2.3 The Mader Problem

The simplest test of detonation is the one-dimensional gamma-law rarefaction wave burn, for which a slab of material is initiated on one side and a detonation propagates to the other side. For a Chapman-Jouget detonation speed of 0.8 cm/μs, it takes 6.25 μs for the detonation to travel 5 cm. The rich structure of a multi-dimensional detonation is absent in the one-dimensional test problem, and a simple rarefaction wave follows the detonation front (Fickett & Davis 1979; Figure 10). Expansion of material in the rarefaction depends on the boundary condition where the detonation is initiated, which is usually modeled as a freely moving surface or a moving piston. For the Mader problem, a stationary piston is used. In this case, the head of the rarefaction remains at the detonation front since the flow is sonic there, and the tail of the rarefaction is halfway between the front and the piston. Care must be taken to use as thin an initiator region as possible in the input deck; otherwise a break in the rarefaction wave occurs (Kirkpatrick, Wingate & Kamm 2004).

Figure 10 shows a representative solution for the density, pressure, and material speed on a 1D uniform mesh of 400 cells at 5.0 μs. These quantities decrease smoothly from the head of the detonation at x=1.0 cm to x=3.0 cm. In this region, the profiles for the density and material speed are linear with position, while the pressure profile is a cubic. Even at a visual level of comparison, one can see differences between the numerical and analytical solutions. In essence, this is because the numerical detonation front does not quite reach x=1.0 cm at 5.0 μs. The dips in the numerical solution at the transition to the constant state may be due to the initiator region being too thick, defined as 2 zones thick for all spatial resolutions (Kirkpatrick, Wingate & Kamm 2004). As the resolution increases the front gets closer to the correct value and the dips disappear.

The parameter he_dtpct sets the maximum relative temperature change allowed per time-step in high explosive material and determines the time-step in the numerical solution of the Mader problem. he_dtpct was set to its default value of 0.1 in Figure 10, limiting temperature changes to a maximum of 10% in one time-step.

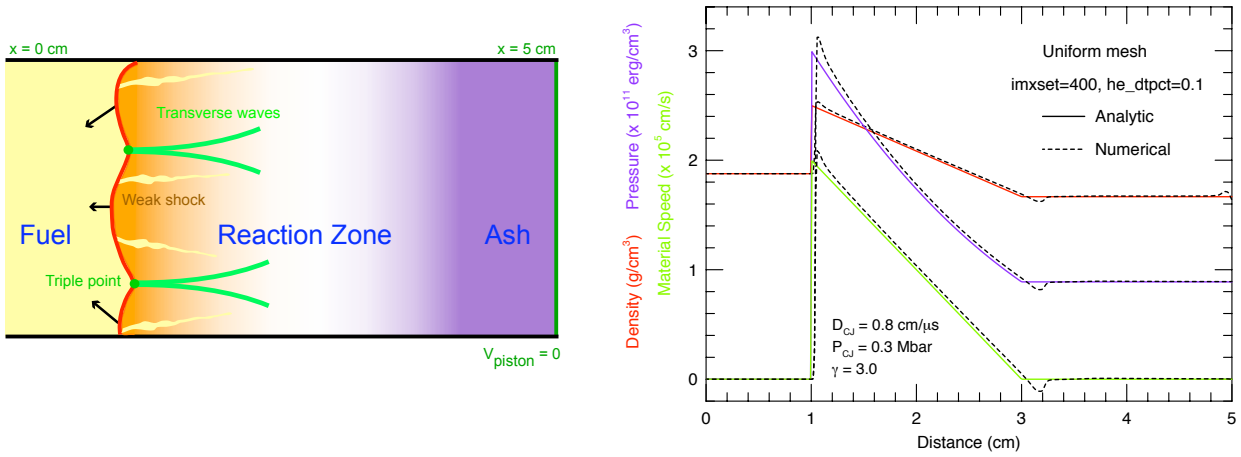

Figure 10. - Setup for the Mader problem is illustrated on the left. On the right are 1D analytical (solid curves) and numerical (dotted curves) solutions at time=5.0 μs for the mass density (red), velocity (green), and pressure (purple). The calculation is for a uniform mesh of 400 cells and a time-step controller of he_dtpct=0.1.

Figure 11 shows the absolute value of the relative errors in the density, pressure, and material speed for 1D uniform grids with 100, 200, 400, 800, 1600, and 3200 cells at the final time of 5.0 μs. The time-step controller was kept at its default value, he_dtpct=0.1. Cusps are due to changes of sign in the relative error, and the relative cpu cost on a single processor of increasing the spatial resolution is shown. Except at the x=1.0 cm detonation front, the errors get smaller with increasing uniform grid resolution.

Failure of the detonation front to reach x=1 cm after 5 μs, may derive from the parameters used in the Forest-Fire model, a global reaction kinetics model for the high-pressure chemical decomposition of heterogeneous explosives (Mader 1997). The Forest-Fire model parameters were supposedly calculated for a uniform grid spacing of 0.025 cm, 200 cells for a 5 cm domain, (Kamm & Kirkpatrick 2004, K. New, private communication 2005). Even at this spatial resolution, the detonation front fails to reach the correct location. At a grid spacing of 0.0015625 cm, or 3200 points, there begins to be sufficient resolution for the detonation to reach the correct position. It is well known, however, that the parameters of Forest-Fire model are cell size and equation of state dependent quantities (Mader 1997), which presents serious difficulties for performing verification studies on different meshes. In addition, we couldn't find anyone who could (or would) state with certainty how the model parameters are to be derived. If the purpose of this test problem in the Tri-Lab Verification Test Suite is to verify detonation wave physics, then there are detonation problems which have far less idiosyncrasies. If the purpose of the test problem is to verify HE burn models, then additional plans are needed to determine how the model parameters are determined.

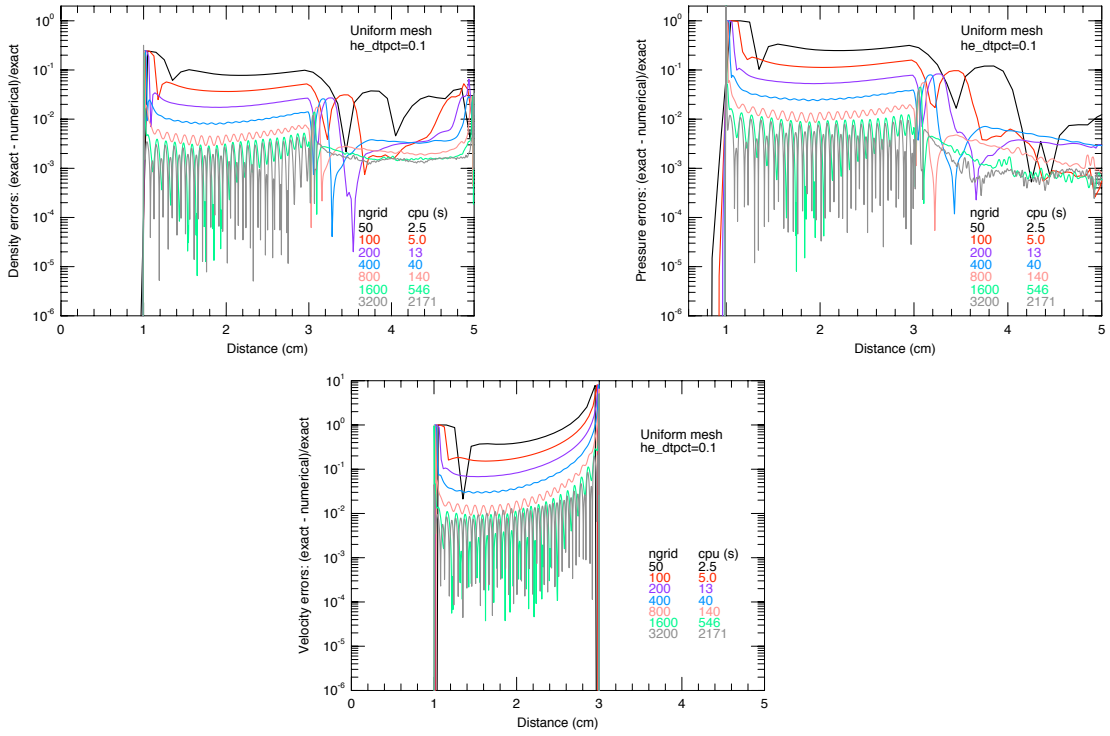

Figure 11. - Absolute value of the relative error in the density (upper left), pressure (upper right), and material speed (lower) at 5.0 μ s for a variety of uniform grids at a fixed time-step control value of he_dtpct=0.1. In general all quantities shown demonstrate linear convergence with spatial resolution.

Table 7
Spatial Convergence Coefficients for the Mader Problem

	Density			Pressure			Speed		
# of cells	$L_{1,abs}$	α	A	$L_{1,abs}$	α	A	$L_{1,abs}$	α	A
100	5.819E-02			1.784E+10			1.427E+04		
200	3.063E-02	9.256E-01	9.313E-01	9.296E+09	9.407E-01	2.988E+11	7.381E+03	9.507E-01	2.461E+05
400	1.649E-02	8.934E-01	8.268E-01	4.787E+09	9.574E-01	3.178E+11	3.791E+03	9.614E-01	2.561E+05
800	8.179E-03	1.012E+00	1.388E+00	2.205E+09	1.118E+00	6.437E+11	1.626E+03	1.221E+00	7.977E+05
1600	3.937E-03	1.055E+00	1.727E+00	8.466E+08	1.381E+00	2.439E+12	5.777E+02	1.493E+00	3.180E+06
3200	2.854E-03	4.644E-01	5.735E-02	4.671E+08	8.580E-01	1.194E+11	4.017E+02	5.242E-01	1.188E+04

Figure 11 suggests, and Table 7 details, that the density, pressure, and material speed all have roughly linear convergence rates that become smaller with increasing spatial resolution at this time-step control setting.

Figure 12 shows absolute value of the relative errors in the density, pressure and material speed for he_dtpct=0.5, 0.2 (the default value), 0.1, 0.05, 0.02, 0.01, and 0.005 on one-dimensional uniform grids of 100 and 400 cells. The relative cpu cost on a single processor of increasing the temporal resolution is shown. Values of he_dtpct $\geq$ 0.2 tend to produce inaccurate results near the detonation front and in the constant-state region x $\geq$ 3.0 cm. Figure 12 suggests and Table 8 shows that the density, pressure and material speed all have a convergence rate of $\beta \sim 0$ at these spatial resolutions. That is, the L_1 norms for Mader problem appear largely independent of the chosen time-step.

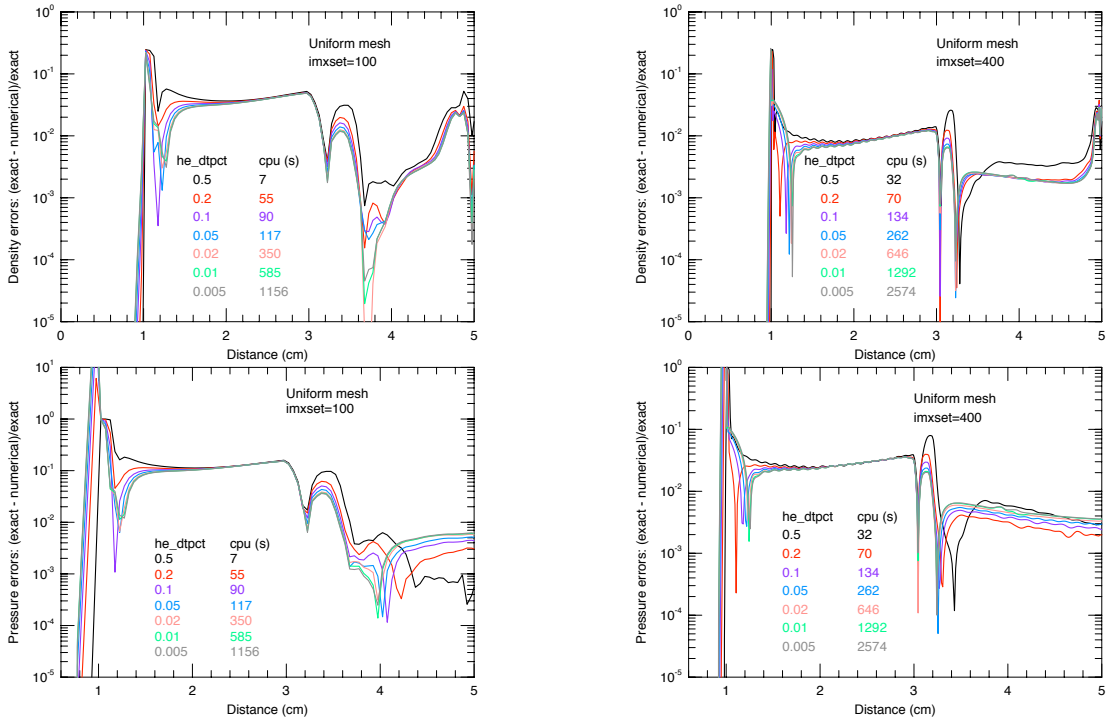

Figure 12. - Absolute value of the relative error in the density (upper), and pressure (lower) for a variety of he_dtpct time-step control values on uniform grids of 100 and 400 cells.

Table 8
Temporal Convergence Coefficients for the Mader Problem

		Density			Pressure			Speed		
ngrid	he_dtpct	$L_{1,abs}$	β	B	$L_{1,abs}$	β	B	$L_{1,abs}$	β	B
100	5.000E-01	5.819E-02			1.784E+10			1.427E+04		
	2.000E-01	4.632E-02	2.490E-01	6.915E-02	1.466E+10	2.144E-01	2.070E+10	1.169E+04	2.176E-01	1.659E+04
	1.000E-01	4.128E-02	1.661E-01	6.051E-02	1.301E+10	1.723E-01	1.934E+10	1.046E+04	1.600E-01	1.512E+04
	5.000E-02	3.880E-02	8.935E-02	5.071E-02	1.200E+10	1.162E-01	1.700E+10	9.782E+03	9.667E-02	1.307E+04
	2.000E-02	3.728E-02	4.376E-02	4.424E-02	1.129E+10	6.673E-02	1.466E+10	9.365E+03	4.760E-02	1.128E+04
	1.000E-02	3.673E-02	2.121E-02	4.050E-02	1.110E+10	2.448E-02	1.243E+10	9.203E+03	2.516E-02	1.033E+04
	5.000E-03	3.646E-02	1.088E-02	3.862E-02	1.102E+10	1.070E-02	1.166E+10	9.121E+03	1.287E-02	9.764E+03
400	5.000E-01	1.649E-02			4.787E+09			3.791E+03		
	2.000E-01	1.190E-02	3.557E-01	2.110E-02	3.280E+09	4.126E-01	6.372E+09	2.611E+03	4.068E-01	5.025E+03
	1.000E-01	1.067E-02	1.573E-01	1.533E-02	2.765E+09	2.464E-01	4.876E+09	2.218E+03	2.351E-01	3.812E+03
	5.000E-02	1.075E-02	-9.699E-03	1.044E-02	2.602E+09	8.749E-02	3.382E+09	2.122E+03	6.389E-02	2.570E+03
	2.000E-02	1.160E-02	-8.327E-02	8.374E-03	2.642E+09	-1.632E-02	2.478E+09	2.261E+03	-6.923E-02	1.725E+03
	1.000E-02	1.202E-02	-5.204E-02	9.462E-03	2.774E+09	-7.050E-02	2.005E+09	2.364E+03	-6.389E-02	1.761E+03
	5.000E-03	1.222E-02	-2.345E-02	1.079E-02	2.852E+09	-4.001E-02	2.307E+09	2.417E+03	-3.199E-02	2.040E+03

Figure 13 shows the $L_{1,abs}$ norms and the residuals of fitting equation (12) to the $L_{1,abs}$ norms of the density, pressure, and material speed when the time-step controller and spatial resolution are varied. The plus signs indicate the spatial and temporal points (the data points) where the $L_{1,abs}$ norm was computed. The images on the left show the $L_{1,abs}$ norm (the data) while the images on the right show the relative residual of fitting the $L_{1,abs}$ norm to the error model (equation 12). If the residuals of the non-linear least squares fitting procedure are small, then the derived convergence rates are probably reliable. Table 9 details the derived spacetime convergence rates. The fitted rates are generally consistent with values derived when the space and time analyses were performed independently, which may be due to our choice of fixing the time-step control value rather than the time-step Δt itself.

Table 9
Spacetime Convergence Rates for the Mader Problem

Parameter	Density	Pressure	Material Speed
A	0.0104093	3.47466e+09	5859.81
α	0.992591	0.9654	0.691861
ngrid_norm	400	400	400
B	0.192962	-2.25693e+11	-2369.33
β	0.0216	-0.00412	-0.220603
he_dtpct_norm	0.05	0.05	0.05
C	-0.191116	2.25295e+11	-1749.3
γ	0.00441394	0.000745	-0.0733634

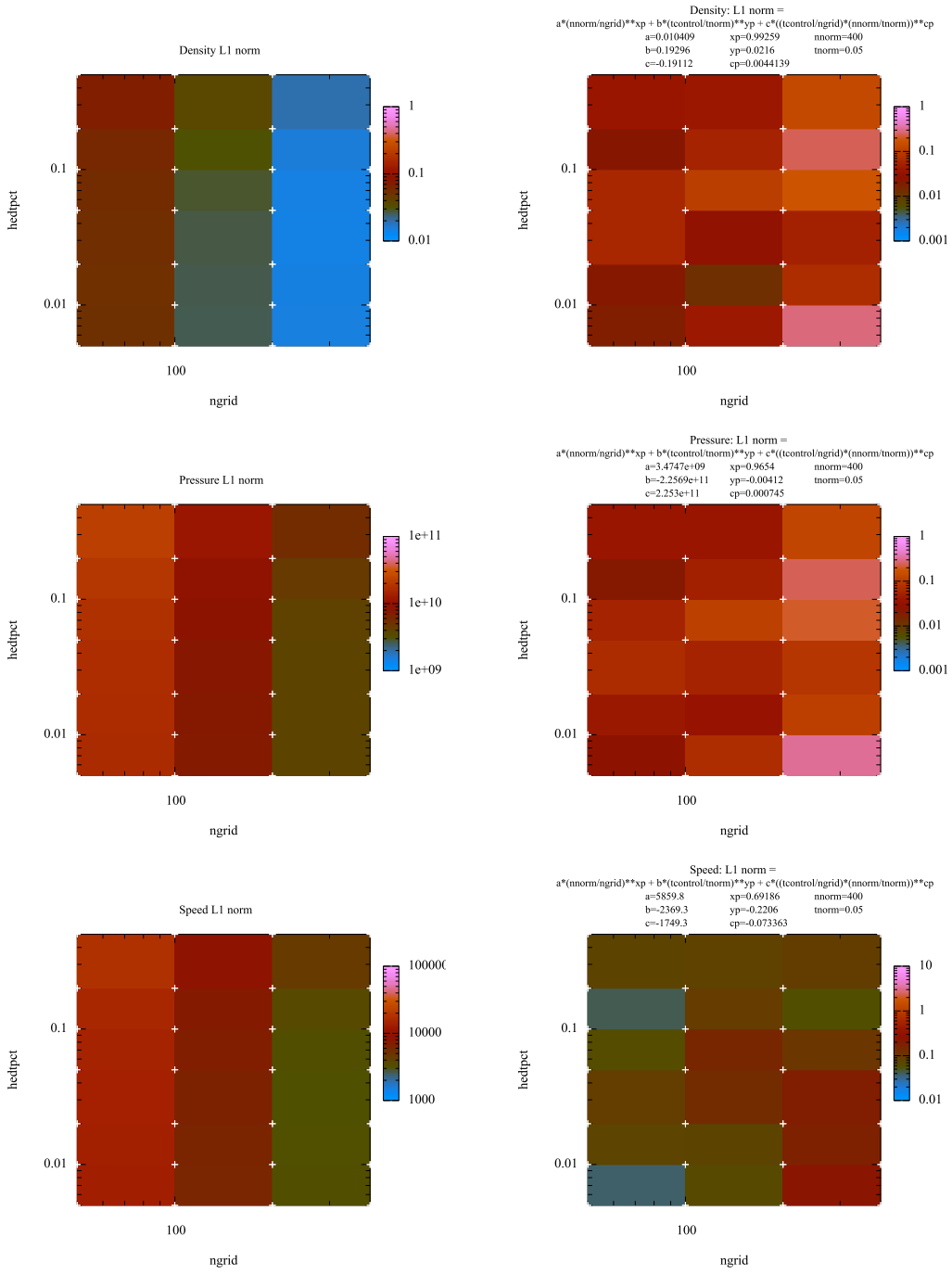

Figure 13. - $L_{1,abs}$ error norms (left) and relative residuals (right) from fitting the error model for the density, pressure, and material speed when spatial and temporal resolution are varied. Plus signs indicate the spacetime points where the error norm was computed.

2.4 The Reinicke & Meyer-ter-Vehn Problem

The Reinicke Meyer-ter-Vehn (1991, henceforth RMTV) problem in the Tri-Lab Verification Test Suite has an initial concentrated energy source of sufficient magnitude so that heat conduction dominates the fluid flow. That is, a thermal front leads a hydrodynamic shock. The other case, where the thermal front lags the hydrodynamic shock is not presently part of the Tri-Lab Suite. RMTV examined the self-similar case and found that the fluid equations reduced to a set of four ordinary differential equations (ODEs). Due to evaluation of the initial conditions and multiple-region integration of the complicated ODEs, the RMTV problem has the distinction of possessing the most complicated `analytical' solution in the Tri-Lab Test Suite. Nevertheless, this problem is useful for verifying time-dependent thermal conduction codes in the presence of shocks (Clover, Kamm, & Rider 2000, Kamm 2000a). A succinct description of the RMTV problem along with fortran code for generating solutions are given by Timmes, Gisler & Hrbek (2005) and are based on the codes used by Kamm (2000a).

A major improvement in 2006 has been an new initialization module for RMTV in RAGE (Timmes & Clover 2006). The new module reduces the size of a RAGE input deck for a 1D version of the RMTV problem by 100 to 3200 lines (See Appendix A). The new module also provides 2D and 3D simulations while D version a more accurate and smoother initial state, which is particularly important for convergence studies on adaptive meshes.

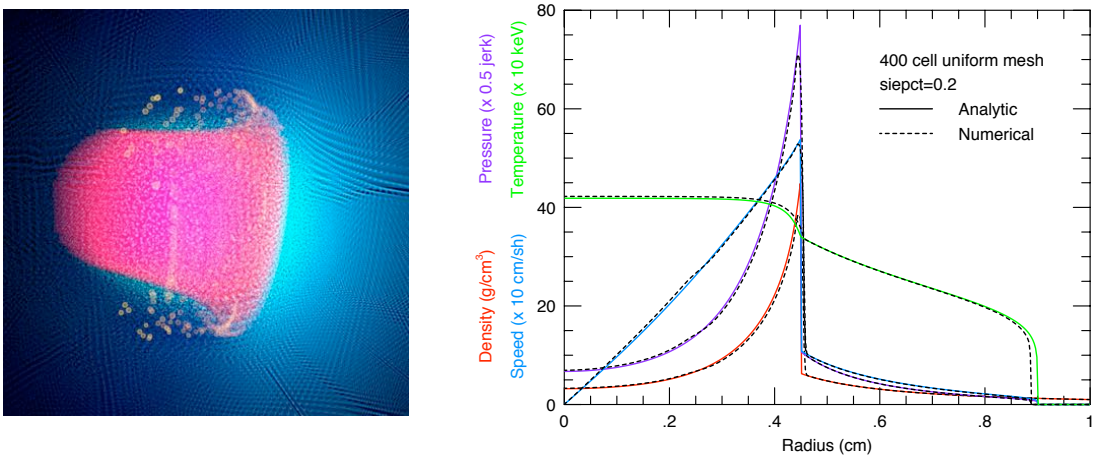

Figure 14. - A smooth particle hydrodynamics visualization of a supercritical shock, where a thermal front leads the hydrodynamic shock is shown on the left. On the right are analytical (solid curves) and numerical (dotted curves) solutions at the final time for the mass density (red), material speed (blue), pressure (purple), and temperature (green). The calculation is for a uniform mesh of 400 cells in 1D spherically symmetric geometry and a time-step controller of siepct=0.2.

Figure 14 shows a representative solution on a 1D uniform mesh of 400 cells. The parameter siepct sets the maximum fractional change in the specific internal energy per time-step. It also determines the time-step in the numerical solution of the RMTV problem and was set at its default value of 0.2, limiting changes in any cell's specific internal energy to 20% in a time-step. Solutions are shown for the density, pressure, temperature, and material

speed at $5.1251245293611 \times 10^{-10}$ s. The analytic and numerical solutions appear reasonable at this level of visual comparison, although there is a difference in the location of the thermal front's leading edge (green curve).

Initialization of the RMTV problem is a critical ingredient. Like the Sedov problem in section 2.6, there can be vigorous debate between depositing all the energy into a single central zone or depositing the energy in a small fixed size region. In Figure 14 the single cell initialization procedure was used, while Figure 15 shows the results of depositing all the energy in a small fixed size region (0.005 cm). Unlike the Sedov problem, however, the results for the RMTV problem are unambiguous: Figures 14 and 15 demonstrate that the energy must be deposited in the single central zone in order to achieve general agreement with the analytic solution.

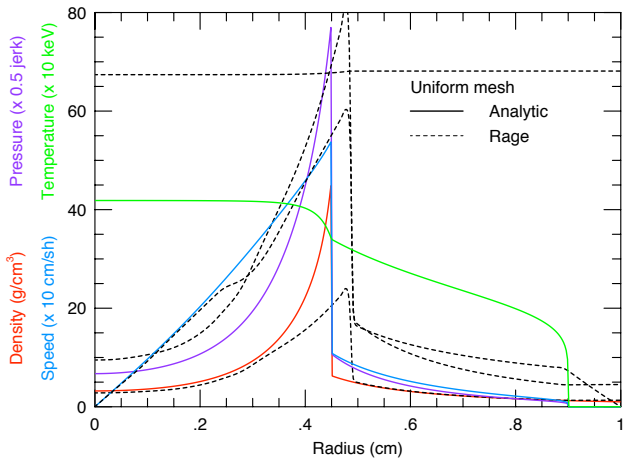

Figure 15. - Solution to the RMTV problem when the initial energy is distributed in a small fixed size region (0.005 cm) rather than in a single cell. The numerical solution isn't even close to the analytic solution. The calculation was performed for the same mesh and time-step controls as Figure 14.

Figure 16 shows the absolute value of the relative errors in the density, pressure, temperature, and material speed for 1D uniform grids with 100, 200, 400, 800, 1600, and 3200 cells at the final time of $5.1251245293611 \times 10^{-10}$ s. The time-step controller was kept at its default value, siepct=0.2. The relative cpu cost on a single processor of increasing the spatial resolution is given. Large persistent errors exist at the leading edge of the thermal front at x=0.9 cm and at the shock front at 0.45 cm. Other cusps are due to changes of sign in the relative error. In the region between the origin and shock at 0.45 cm the errors generally decrease with increasing spatial resolution, but fail to follow a clear pattern. In the region between the shock front at 0.45 cm and the thermal front at 0.90 cm the errors associated with the density solution saturate, but the temperature and velocity errors increase (!) with increasing resolution.

Figure 16 and Table 10 show that the $L_{1,abs}$ norms of the density, pressure, temperature, and material speed all have roughly square-root convergence rates ($\alpha \sim 0.5$) with spatial resolution at this time-step control setting. The temperature converges more slowly because of the larger errors near the leading of the thermal front that slowly get smaller as more grid is added.

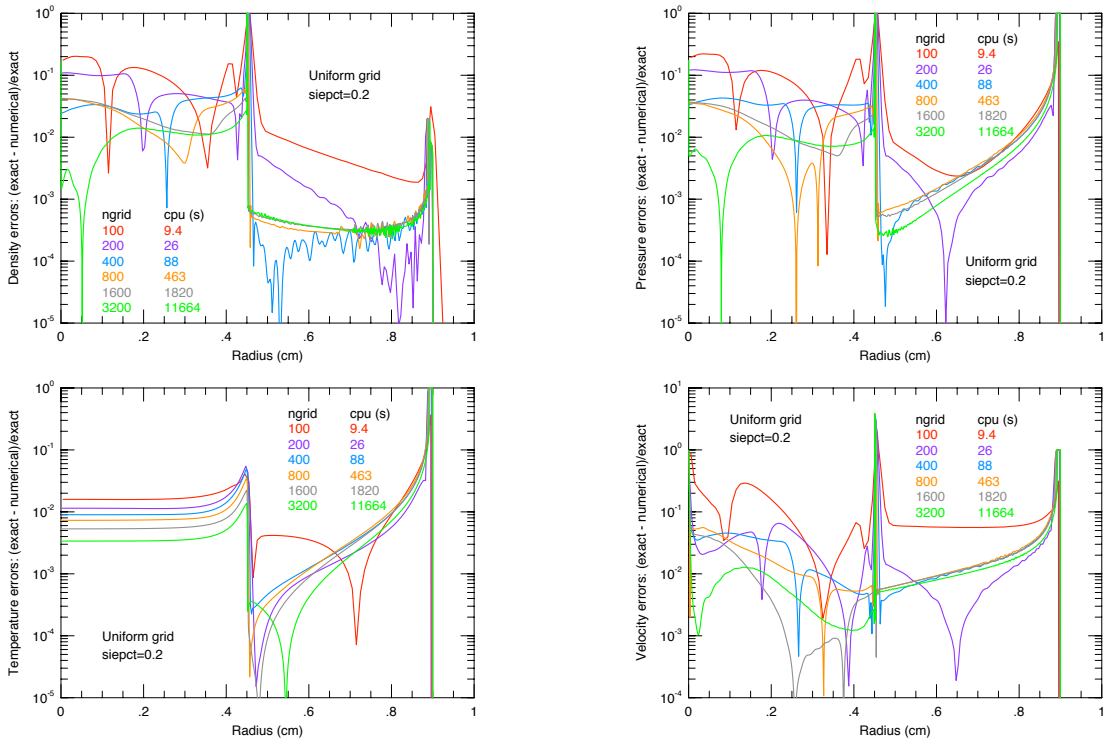

Figure 16. - Absolute value of the relative error in the density (upper left), pressure (upper right), temperature (lower left) and material speed (lower right) for a variety of uniform meshes at a fixed time-step controller siepct=0.2. In general all quantities shown demonstrate a square-root convergence rate with spatial resolution.

Table 10
Spatial Convergence Coefficients for the RMTV Problem

	Density			Pressure		
# of cells	$L_{1,abs}$	α	A	$L_{1,abs}$	α	A
100	2.741E-01			1.044E+16		
200	1.748E-01	6.490E-01	5.443E+00	6.237E+15	7.429E-01	3.194E+17
400	1.657E-01	7.692E-02	2.628E-01	5.687E+15	1.332E-01	1.263E+16
800	1.208E-01	4.559E-01	2.544E+00	4.190E+15	4.406E-01	7.968E+16
1600	7.978E-02	5.989E-01	6.621E+00	2.827E+15	5.677E-01	1.863E+17
3200	5.107E-02	6.435E-01	9.200E+00	1.869E+15	5.971E-01	2.315E+17
	Temperature			Speed		
# of cells	$L_{1,abs}$	α	A	$L_{1,abs}$	α	A
100	3.403E+01			4.907E+06		
200	5.596E+01	-7.176E-01	1.250E+00	2.834E+06	7.923E-01	1.886E+08
400	5.593E+01	8.225E-04	5.620E+01	2.331E+06	2.819E-01	1.262E+07
800	5.206E+01	1.034E-01	1.039E+02	1.787E+06	3.828E-01	2.310E+07
1600	4.404E+01	2.413E-01	2.613E+02	1.228E+06	5.412E-01	6.660E+07
3200	3.337E+01	4.003E-01	8.441E+02	8.910E+05	4.632E-01	3.744E+07

Figure 17 shows absolute value of the relative errors in the density, and temperature for siepct=0.4, 0.2 (the default value), 0.1, 0.05, 0.02, on 0.01 on one-dimensional uniform grids of 100 and 800 cells. The relative cpu cost on a single processor of increasing the temporal resolution is shown. Figure 17 shows and Table 11 confirms the density, pressure, temperature, and material speed all have a convergence rate of $\beta \sim 0$ at these spatial resolutions. That is, the L_1 norms for RMTV problem appear largely independent of the chosen time-step. This suggests that spatial errors, particularly for less than 800 cells, dominate the error budget.

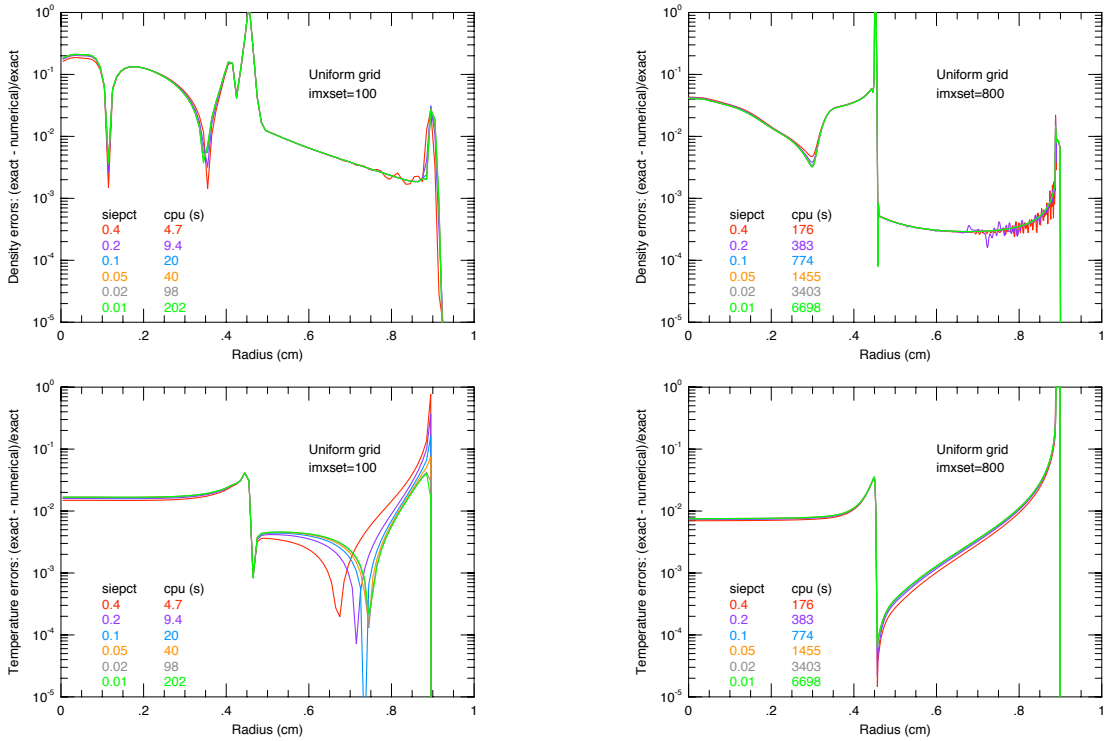

Figure 17. - Absolute value of the relative error in the density (upper) and temperature (lower) for a variety of time-step control values on meshes with 100 and 800 cells. In general, the time-step shows a zeroth order of convergence for all quantities.

Figure 18 shows the $L_{1,abs}$ norms and the residuals of fitting equation (12) to the $L_{1,abs}$ norms of the density, temperature, pressure, and material speed when the time-step controller and spatial resolution are varied. The plus signs indicate the spatial and temporal points (the data points) where the $L_{1,abs}$ norm was computed. The images on the left show the $L_{1,abs}$ norm (the data) while the images on the right show the relative residual of fitting the $L_{1,abs}$ norm to the error model (equation 12). If the residuals of the non-linear least squares fitting procedure are small, then the derived convergence rates are probably reliable. Table 12 details the derived spacetime convergence rates. The fitted rates are generally consistent with values derived when the space and time analyses were performed independently because the $\Delta x \Delta t$ cross-terms have relatively small coefficients and exponents in this regime.

Table 11
Temporal Convergence Coefficients for the RMTV Problem

		Density			Pressure		
ngrid	siepct	$L_{1,abs}$	β	B	$L_{1,abs}$	β	B
100	4.000E-01	6.063E-01			2.351E+16		
	2.000E-01	6.184E-01	-2.858E-02	5.906E-01	2.396E+16	-2.711E-02	2.293E+16
	1.000E-01	6.228E-01	-1.032E-02	6.082E-01	2.413E+16	-1.032E-02	2.356E+16
	5.000E-02	6.249E-01	-4.648E-03	6.162E-01	2.421E+16	-4.895E-03	2.386E+16
	2.000E-02	6.265E-01	-2.878E-03	6.195E-01	2.428E+16	-3.016E-03	2.399E+16
	1.000E-02	6.268E-01	-7.597E-04	6.246E-01	2.429E+16	-9.505E-04	2.419E+16
800	4.000E-01	2.429E-01			7.406E+15		
	2.000E-01	2.408E-01	1.259E-02	2.457E-01	7.310E+15	1.880E-02	7.534E+15
	1.000E-01	2.397E-01	6.787E-03	2.434E-01	7.258E+15	1.020E-02	7.431E+15
	5.000E-02	2.393E-01	2.169E-03	2.408E-01	7.240E+15	3.722E-03	7.321E+15
	2.000E-02	2.391E-01	7.756E-04	2.398E-01	7.231E+15	1.282E-03	7.267E+15
	1.000E-02	2.391E-01	3.017E-04	2.394E-01	7.228E+15	5.987E-04	7.248E+15

		Temperature			Speed		
ngrid	siepct	$L_{1,abs}$	β	B	$L_{1,abs}$	β	B
100	4.000E-01	5.206E+01			1.196E+07		
	2.000E-01	4.697E+01	1.483E-01	5.964E+01	1.213E+07	-2.084E-02	1.173E+07
	1.000E-01	4.428E+01	8.505E-02	5.386E+01	1.216E+07	-3.920E-03	1.205E+07
	5.000E-02	4.317E+01	3.666E-02	4.818E+01	1.218E+07	-2.015E-03	1.211E+07
	2.000E-02	4.260E+01	1.456E-02	4.510E+01	1.221E+07	-2.595E-03	1.209E+07
	1.000E-02	4.244E+01	5.327E-03	4.350E+01	1.221E+07	-3.545E-04	1.219E+07
800	4.000E-01	3.669E+01			3.022E+06		
	2.000E-01	3.763E+01	-3.650E-02	3.548E+01	3.032E+06	-4.814E-03	3.008E+06
	1.000E-01	3.810E+01	-1.783E-02	3.656E+01	3.034E+06	-1.142E-03	3.026E+06
	5.000E-02	3.831E+01	-8.232E-03	3.738E+01	3.035E+06	-4.279E-04	3.031E+06
	2.000E-02	3.844E+01	-3.470E-03	3.792E+01	3.036E+06	-4.674E-04	3.031E+06
	1.000E-02	3.848E+01	-1.501E-03	3.821E+01	3.037E+06	-1.425E-04	3.035E+06

Table 12
Spacetime Convergence Rates for the RMTV Problem

Parameter	Density	Pressure	Temperature	Material Speed
A	0.219551	1.30684e+16	10.2395	6.23156e+06
α	0.612	0.489	0.312	0.546
ngrid_norm	400	400	400	400
B	0.0499217	1.21641e+16	108.993	8.45031e+06
β	-0.00216	-0.0007301	-0.0004213	-0.000778
siepct_norm	0.1	0.1	0.1	0.1
C	0.0439597	-1.47473e+16	-77.0865	-1.04085e+07
γ	0.001	0.002228	0.001278	0.0005219

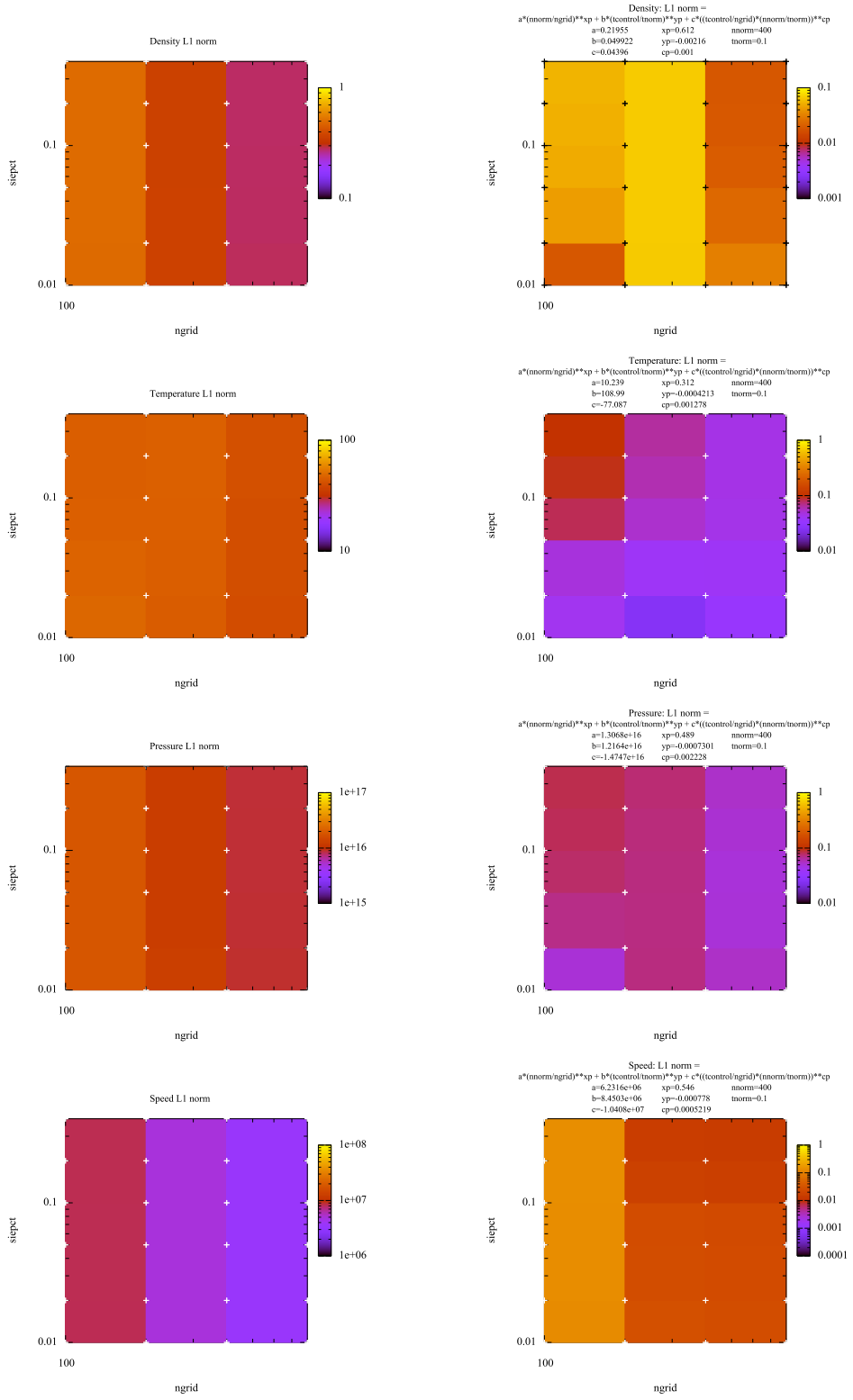

Figure 18. - $L_{1,abs}$ error norms (left) and relative residuals (right) from fitting the error model for the density, pressure, and material speed when spatial and temporal resolution are varied. Plus signs indicate the spacetime points where the error norm was computed.

2.5 The Noh Problem

The Noh problem (Noh 1987) is a standard verification problem for hydrocodes. A gamma-law gas is initialized with a uniform, radially inward velocity. A shock forms at the origin and propagates outward as the gas stagnates. This problem tests a code's ability to transform kinetic energy into internal energy, and the ability to follow supersonic flows. The analytical solution is easy to calculate, and the convergence of the hydrocode solution can be directly determined. A description of the solution to the Noh problem, along with fortran code for generating solutions, is given by Timmes, Gisler & Hrbek (2005).

Figure 19 compares the analytical and numerical solutions for the density, pressure, temperature and material speed on a 800 cell uniform grid. The parameter tstab sets the time step allowed by the material speed, Δt = tstab · Δx / ($|v_x| + |v_y| + |v_z|$), and determines the time-step in the numerical solution of the Noh problem. It was set at its default value of 0.2, limiting transport to 20% of a cell's width.

Shock reflection or shock interactions are often associated with a phenomenon known generically as wall heating (Noh 1987). RAGE, like most other hydrodynamics codes, produces the anomaly when reflecting a shock off a boundary or focusing a shock toward the origin in a convergent geometry (Rider 2000). This heating causes premature stagnation, with densities lower than predicted in the centermost cells. In Figure 19 the central zones has a stagnation density above 75 g/cc. Further out, matter stagnates at densities of 58-62 g cm^{-3}. The correct value is 64 g cm^{-3}. The extent to which the anomalous heating occurs depends on the nature of the shock reflection, so that wall heating may or may not be important for a given problem.

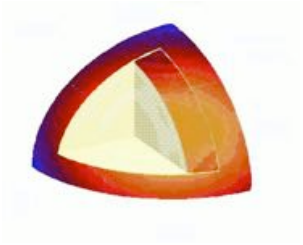

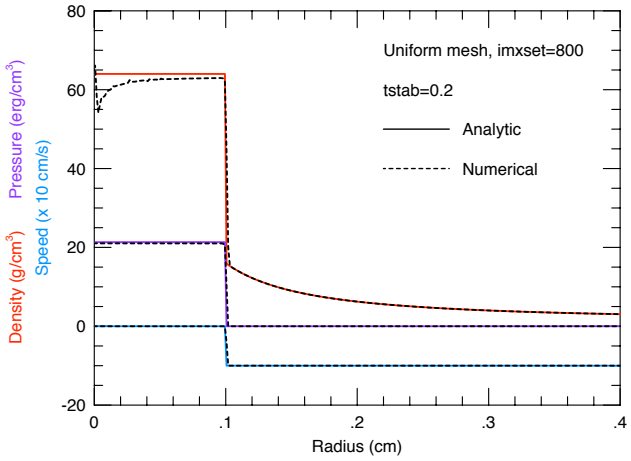

Figure 19. - An illustration of the Noh problem in 3D is shown on the left. On the right are analytical (solid curves) and numerical (dotted curves) solutions at 0.3 s for the mass density (red), material speed (blue) and pressure (purple).

Figure 20 shows the absolute value of the relative errors in the density, pressure, temperature, and material speed for uniform grids with 100, 200, 400, 800, 1600, and 3200 cells at the final time of 0.3 s. The time-step controller was kept at its default value, tstab=0.2. The relative cpu cost on a single processor of increasing the spatial resolution is given. Note the density plot has a different x-axis scale. The large errors from the anomalous heating at the

origin is evident. Persistent errors near the right boundary are probably due to the inflow boundary condition. It is encouraging, however, that between the origin and the shock there is a steady decline in the magnitude of the errors as the spatial resolution is increased.

Figure 20 and Table 13 show that the density, pressure, and material speed have roughly linear convergence rates ($\alpha \sim 1$), mainly due to the large persistent errors from wall-heating and the inflow boundary at this time-step control setting.

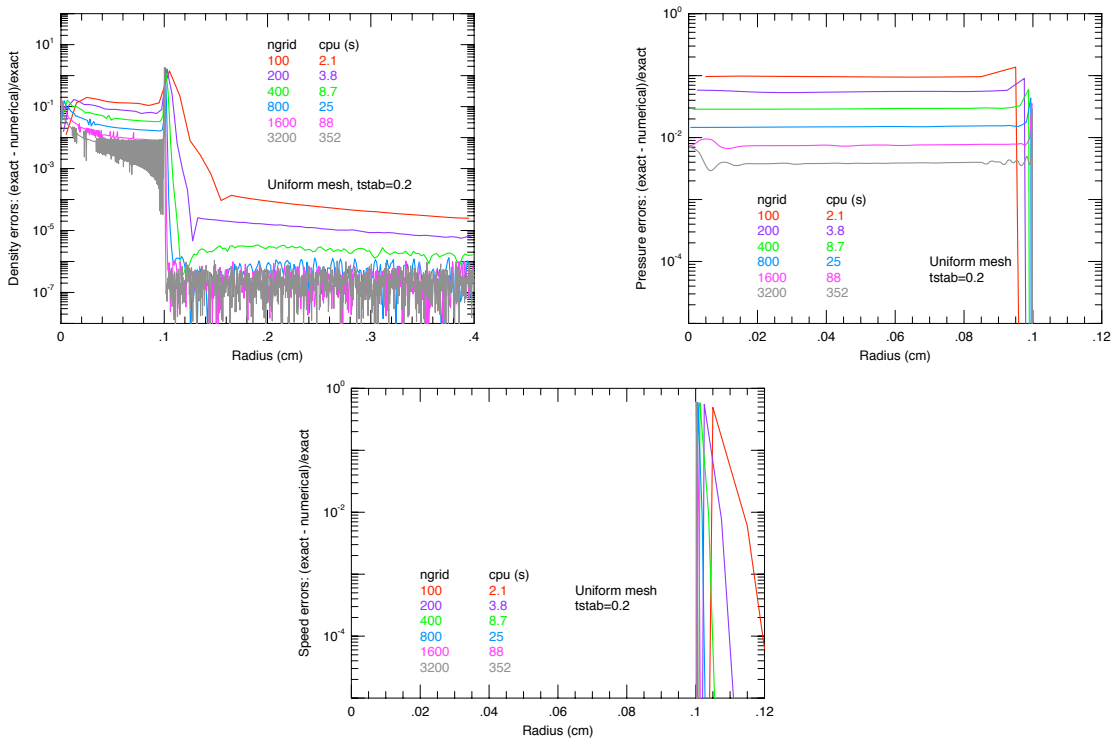

Figure 20. - Absolute value of the relative error in the density (upper left), pressure (upper right), and material speed (lower middle) for a variety of uniform meshes at a fixed time-step controller tstab=0.2. In general, the quantities shown demonstrate a linear convergence rate with spatial resolution.

Table 13
Spatial Convergence Coefficients for the Noh Problem

	Density			Pressure			Speed		
# of cells	$L_{1,abs}$	α	A	$L_{1,abs}$	α	A	$L_{1,abs}$	α	A
100	2.588E-01			7.344E-02			2.707E-03		
200	1.456E-01	8.297E-01	1.182E+01	4.261E-02	7.856E-01	2.736E+00	1.446E-03	9.043E-01	1.742E-01
400	7.723E-02	9.148E-01	1.855E+01	2.268E-02	9.099E-01	5.287E+00	7.426E-04	9.615E-01	2.358E-01
800	3.945E-02	9.691E-01	2.568E+01	1.163E-02	9.634E-01	7.286E+00	3.735E-04	9.915E-01	2.824E-01
1600	1.967E-02	1.004E+00	3.244E+01	5.836E-03	9.946E-01	8.976E+00	1.852E-04	1.012E+00	3.241E-01
3200	1.001E-02	9.739E-01	2.597E+01	2.972E-03	9.734E-01	7.672E+00	9.398E-05	9.785E-01	2.529E-01

Figure 21 shows absolute value of the relative errors in the density for tstab=0.8, 0.6, 0.4, 0.2 (the default value), 0.1, 0.05, 0.02, on 0.01 on one-dimensional uniform grids of 100 and 1600 cells. The relative cpu cost on a single processor of increasing the temporal resolution is shown. Figure 21 and Table 14 show that the density has a bimodal convergence rate. For tstab≥0.2 the convergence rate in the $L_{1,abs}$ norm is near linear, while for smaller values of tstab the convergence rate is near zero. That is, the L_1 norm for the Noh problem appears largely independent of the chosen time-step below a certain level.

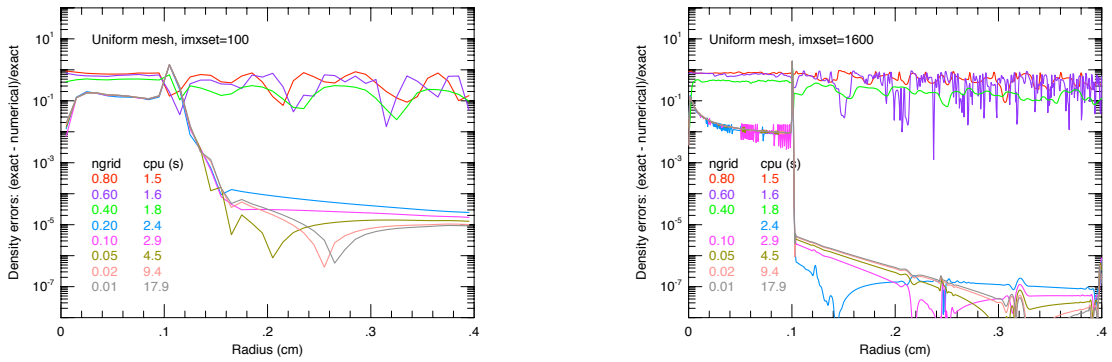

Figure 21. - Absolute value of the relative error in the density for a variety of time-step control values on meshes with 100 and 1600 cells. In general, the time-step shows a near linear convergence rate above tstab=0.2 and a near zeroth order of convergence for smaller values of tstab.

Table 14
Temporal Convergence Coefficients for the Noh Problem

		Density			Pressure			Speed		
ngrid	tstab	$L_{1,abs}$	β	B	$L_{1,abs}$	β	B	$L_{1,abs}$	β	B
100	8.000E-01	2.578E+00			2.973E-01			9.493E-03		
	6.000E-01	2.304E+00	3.900E-01	2.812E+00	2.551E-01	5.310E-01	3.347E-01	6.722E-03	1.200E+00	1.241E-02
	4.000E-01	1.310E+00	1.394E+00	4.696E+00	1.928E-01	6.911E-01	3.632E-01	3.961E-03	1.304E+00	1.309E-02
	2.000E-01	2.588E-01	2.339E+00	1.117E+01	7.344E-02	1.392E+00	6.906E-01	2.707E-03	5.495E-01	6.554E-03
	1.000E-01	2.698E-01	-6.027E-02	2.349E-01	7.781E-02	-8.333E-02	6.422E-02	2.847E-03	-7.311E-02	2.406E-03
	5.000E-02	2.735E-01	-1.965E-02	2.579E-01	7.956E-02	-3.218E-02	7.225E-02	2.895E-03	-2.397E-02	2.694E-03
	2.000E-02	2.761E-01	-1.005E-02	2.654E-01	8.060E-02	-1.413E-02	7.627E-02	2.927E-03	-1.218E-02	2.791E-03
	1.000E-02	2.775E-01	-7.454E-03	2.681E-01	8.103E-02	-7.605E-03	7.824E-02	2.941E-03	-6.540E-03	2.854E-03
1600	8.000E-01	2.954E+00			2.628E-01			1.269E-03		
	6.000E-01	2.483E+00	6.028E-01	3.379E+00	2.300E-01	4.632E-01	2.914E-01	1.333E-03	-1.718E-01	1.221E-03
	4.000E-01	1.197E+00	1.801E+00	6.230E+00	1.480E-01	1.088E+00	4.009E-01	6.762E-04	1.675E+00	3.137E-03
	2.000E-01	1.965E-02	5.928E+00	2.735E+02	5.833E-03	4.665E+00	1.064E+01	1.851E-04	1.869E+00	3.749E-03
	1.000E-01	2.145E-02	-1.259E-01	1.605E-02	6.455E-03	-1.463E-01	4.609E-03	2.075E-04	-1.650E-01	1.419E-04
	5.000E-02	2.197E-02	-3.482E-02	1.979E-02	6.640E-03	-4.077E-02	5.877E-03	2.145E-04	-4.767E-02	1.859E-04
	2.000E-02	2.235E-02	-1.852E-02	2.079E-02	6.764E-03	-2.013E-02	6.251E-03	2.191E-04	-2.366E-02	1.998E-04
	1.000E-02	2.243E-02	-5.413E-03	2.188E-02	6.792E-03	-6.066E-03	6.605E-03	2.201E-04	-6.240E-03	2.139E-04

Figure 22 shows the $L_{1,abs}$ norms and the residuals of fitting equation (12) to the $L_{1,abs}$ norms of the density, temperature, pressure, and material speed when both the time-step controller and spatial resolution are varied. The plus signs indicate the spatial and temporal points (the data points) where the $L_{1,abs}$ norm was computed. The images on the left show the $L_{1,abs}$ norm (the data) while the images on the right show the relative residual of fitting the $L_{1,abs}$ norm to the error model (equation 12). If the residuals of the non-linear least squares fitting procedure are small, then the derived convergence rates are probably reliable. Table 15 details the derived spacetime convergence rates. The fitted rates are generally consistent with values derived when the space and time analyses were performed independently because the $\Delta x \Delta t$ cross-terms have relatively small coefficients and exponents in this regime.

Table 15
Spacetime Convergence Rates for the Noh Problem

Parameter	Density	Pressure	Material Speed
A	0.096083	0.0298196	0.000888175
α	0.779759	0.739461	0.858912
ngrid_norm	400	400	400
B	11.7329	4.30684	0.354423
β	-0.000267	-0.000277	-0.00012
tstab_norm	0.05	0.05	0.05
C	-11.7451	-4.31148	-0.354488
γ	-2.52e-05	-2.17e-05	-1.56e-05

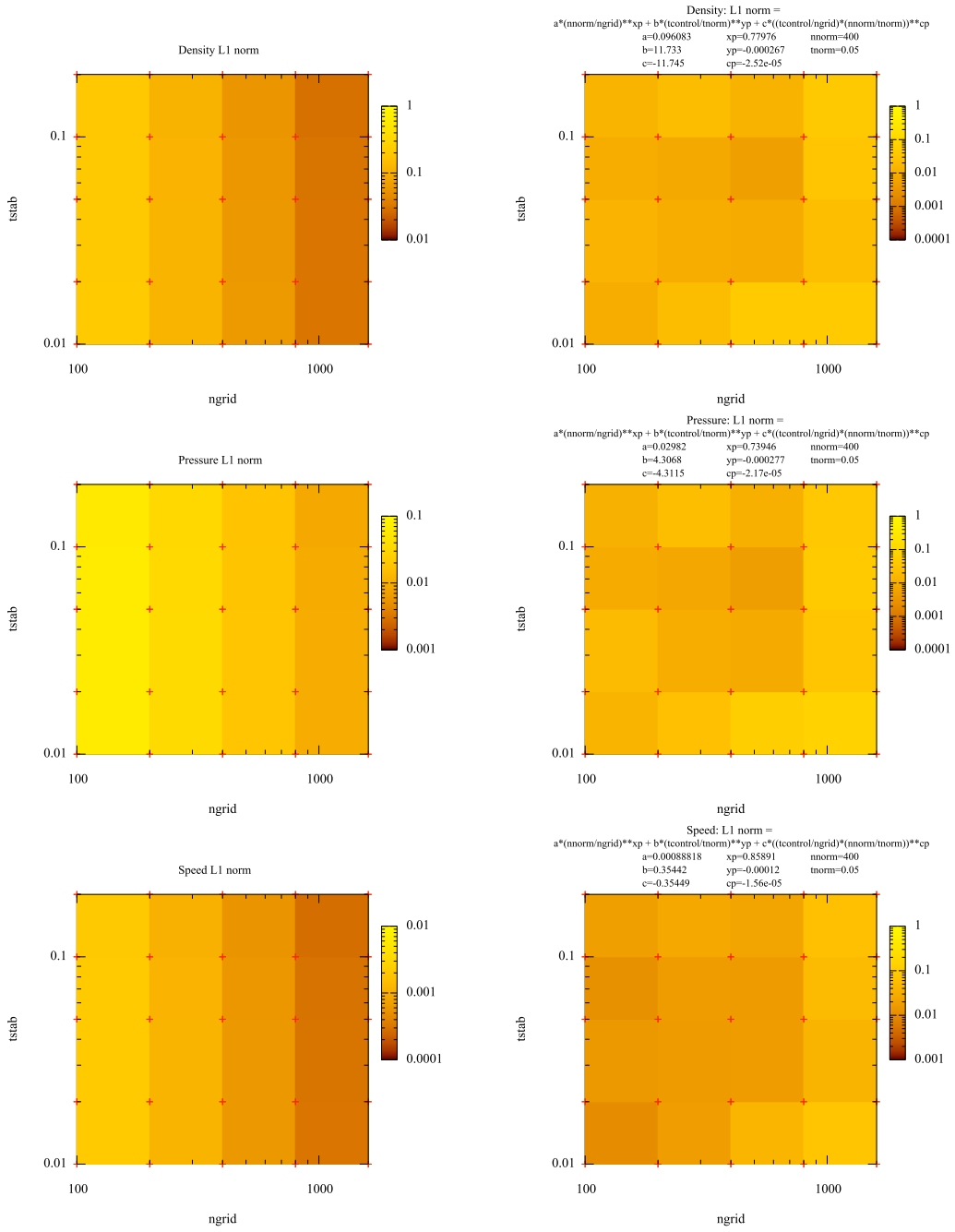

Figure 22. - $L_{1,abs}$ error norms (left) and relative residuals (right) from fitting the error model for the density, pressure, and material speed when spatial and temporal resolution are varied. Plus signs indicate the spacetime points where the error norm was computed.

2.6 The Sedov Problem

A finite amount of energy is deposited at the origin at an initial time. The problem of finding self-similar, one-dimensional solutions for compressible hydrodynamics was considered by Sedov (1959), Taylor (1950), and von Neumann (1947). Sedov provided the most general closed-form solution, which we employ in the forms considered by Kamm (2000b). A description of the solution to the Sedov problem, including regularization of the singularities at the lower limits of integration and fortran code for generating solutions, is given by Timmes, Gisler & Hrbek (2005).

Figure 23 compares the analytical and numerical solutions for the density, pressure, temperature and material speed on a 800 cell uniform grid. The parameter cstab sets the time-step based on the local sound speed and the material velocity, Δt = cstab $\cdot$ Δx / (c + max($|v_x| + |v_y| + |v_z|$)), and determines the time-step in the numerical solution of the Sedov problem. It was set at its default value of 0.9, limiting the time-step to a sound wave crossing 90% of a cell width.

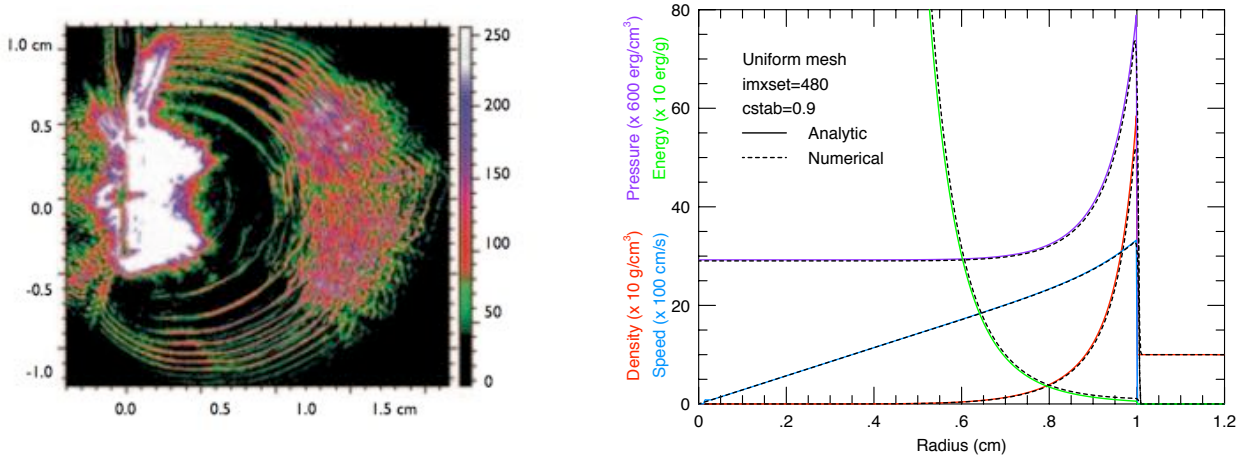

Figure 23. - A multiple-frame shadowgraph of a blast wave initiated by the Trident laser explores the stability of a Taylor-Sedov blast wave (left). On the right are analytical (solid curves) and numerical (dotted curves) solutions at 1.0 s for the mass density (red), material speed (blue), pressure (purple), and specific internal energy (green). The calculation is for a uniform mesh of 480 cells in 1D spherically symmetric geometry and a time-step controller of cstab=0.9.

Initialization of the Sedov problem typically generates a spirited discussion whose antagonists are divided between depositing all the energy into a single central zone or depositing the energy in a small fixed size region. While the one-cell case is perhaps a more authentic way of initializing the problem, it is rarely seen in the refereed literature (Reile & Gehren 1991; Buchler et al 1997; Fryxell et al. 2000; although see Swesty & Myra 2006). Figure 24 shows the numerical solutions for the two cases along with the analytical solution at the final time of 1.0 s. The single cell initialization took 95281 time-steps and the small fixed region (0.02 cm) initialization took 11873 time-steps. For $r > 0.3$ the differences between the specific internal energy for the two cases is small and generally agrees with the analytic solution. For $r < 0.3$ the differences between the two cases becomes substantially worse as the origin is

approached. Neither case agrees with the analytic solution, although the single cell initialization is closer. Similar comments hold for the density. In contrast, the pressure and material speed solutions for the two cases generally agree with the analytic solution as $r \rightarrow 0$.

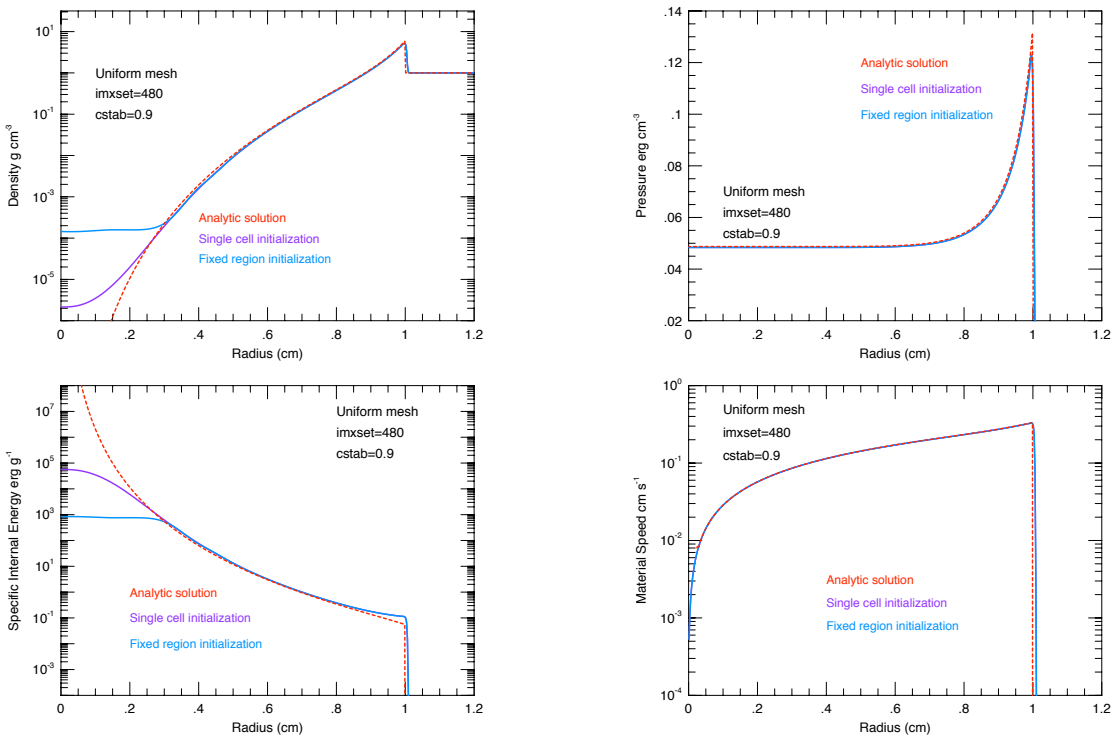

Figure 24. - Comparison of the solutions to the Sedov problem for the density (upper left), pressure (upper right), specific internal energy (lower left), and material speed (lower right) when the initial energy is deposited in an exact delta-function (red curve), in a single cell (purple), and in a small fixed size region (blue) at the final time of 1.0 s.

Figure 25 shows the absolute value of the relative errors in the density, pressure, specific internal energy, and material speed for 1D uniform grids with 120, 240, 480, 960, 1920, and 3840 cells at the final time of 1.0 s. The single cell initialization procedure was used. The time-step controller was kept at its default value, cstab=0.9. The relative cpu cost on a single processor of increasing the spatial resolution is given. The singularity at the origin means T($r \rightarrow 0$) $\rightarrow \infty$, implying large errors in the specific energy near the origin. With the exception of the specific internal energy, there is a steady decline in the magnitude of the errors between the origin and the shock front as the spatial resolution is increased. Figure 25 and Table 16 show that the density, pressure, and material speed have roughly linear convergence rates ($\alpha \sim 1$), while the specific internal energy has a near zero convergence rate (because of the persistent errors at the origin). For the fixed region initialization procedure we find the same convergence rates to within 2 significant figures (see Figure 24).

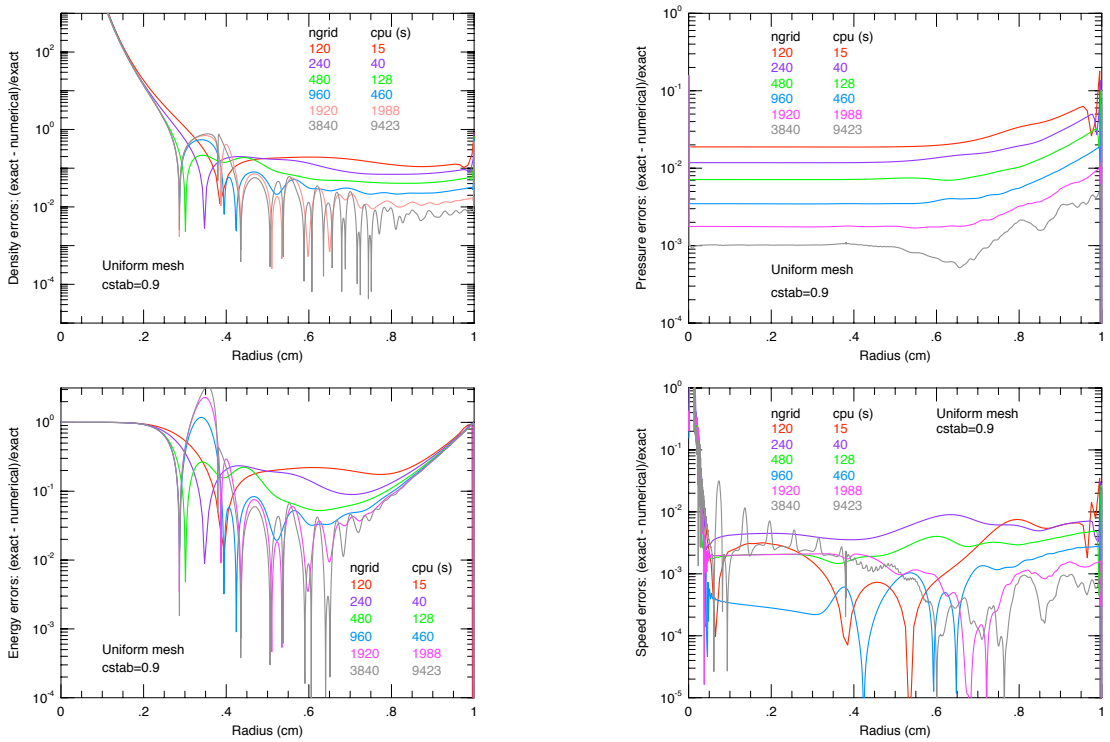

Figure 25. - Absolute value of the relative error in the density (upper left), pressure (upper right), energy (lower left), and material speed (lower right) for a variety of uniform meshes at a fixed time-step controller cstab=0.9. In general, the density, pressure, and material speed show a linear convergence rate with spatial resolution at this value of the time-step controller.

Table 16
Spatial Convergence Coefficients for the Sedov Problem

	Density			Pressure			Speed		
# of cells	$L_{1,abs}$	α	A	$L_{1,abs}$	α	A	$L_{1,abs}$	α	A
120	1.594E-01			3.575E-03			8.700E-03		
240	1.042E-01	6.133E-01	2.687E+00	2.359E-03	5.995E-01	5.653E-02	5.586E-03	6.391E-01	1.651E-01
480	6.066E-02	7.807E-01	6.520E+00	1.372E-03	7.822E-01	1.488E-01	3.104E-03	8.476E-01	4.983E-01
960	3.296E-02	8.799E-01	1.182E+01	7.446E-04	8.817E-01	2.701E-01	1.633E-03	9.271E-01	8.024E-01
1920	1.723E-02	9.360E-01	1.719E+01	3.887E-04	9.376E-01	3.925E-01	8.594E-04	9.258E-01	7.953E-01
3840	8.839E-03	9.629E-01	2.097E+01	1.983E-04	9.710E-01	5.022E-01	4.443E-04	9.517E-01	9.630E-01

Figure 26 shows absolute value of the relative errors in the density and material speed for cstab=0.99, 0.95, 0.9 (the default value), 0.7, 0.5, 0.3, on 0.1 on one-dimensional uniform grids of 240 and 960 cells. The single cell initialization procedure was used. The relative cpu cost on a single processor of increasing the temporal resolution is shown. Figure 26 and Table 17 show these quantities have a convergence rate near zero. That is, the L_1 norm for the Sedov problem appears largely independent of the chosen time-step, which suggests that the spatial discretization may dominate the error budget.

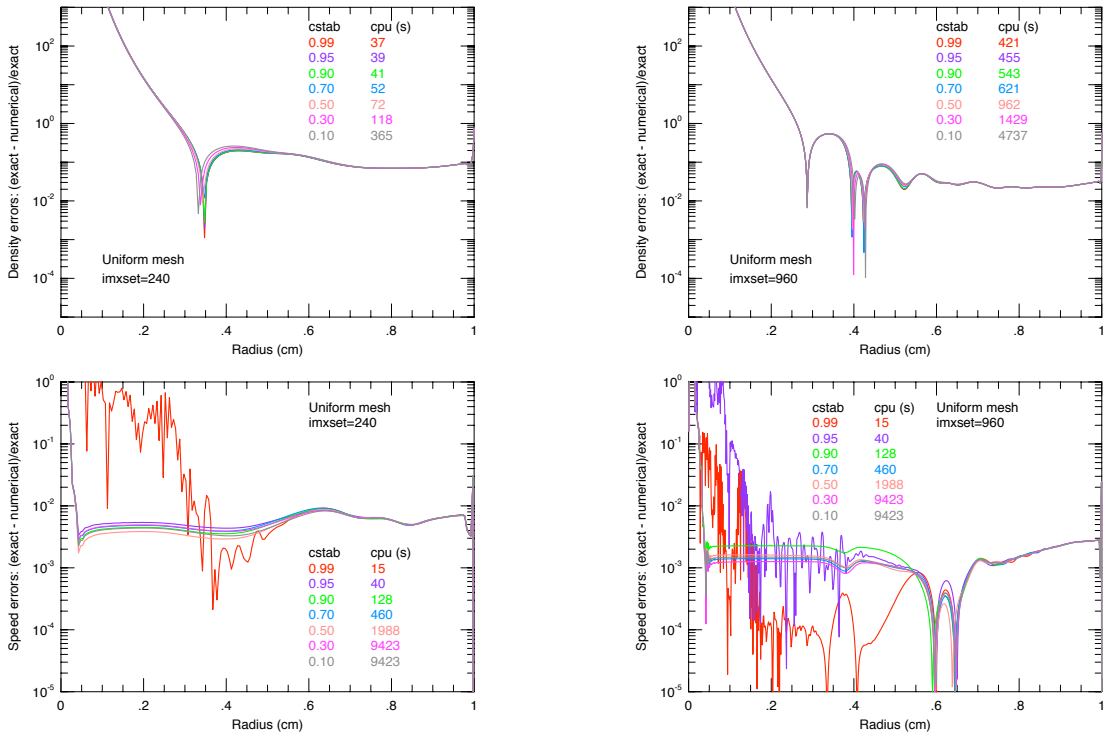

Figure 26. - Absolute value of the relative error in the density and material speed for a variety of time-step control values on meshes with 240 and 960 cells. In general, there is a near zeroth order of convergence with cstab, suggesting spatial errors dominate the error budget.

Table 17
Temporal Convergence Coefficients for the Sedov Problem

		Density			Pressure			Speed		
ngrid	cstab	$L_{1,abs}$	β	B	$L_{1,abs}$	β	B	$L_{1,abs}$	β	B
240	9.900E-01	5.358E-02			1.504E-03			1.018E-02		
	9.500E-01	5.356E-02	7.242E-03	5.358E-02	1.507E-03	-3.704E-02	1.504E-03	3.064E-03	2.911E+01	1.364E-02
	9.000E-01	5.358E-02	-4.834E-03	5.355E-02	1.506E-03	1.351E-02	1.508E-03	3.043E-03	1.290E-01	3.085E-03
	7.000E-01	5.363E-02	-3.934E-03	5.355E-02	1.505E-03	2.643E-04	1.506E-03	3.062E-03	-2.503E-02	3.035E-03
	5.000E-01	5.365E-02	-1.385E-03	5.360E-02	1.503E-03	4.939E-03	1.508E-03	3.019E-03	4.233E-02	3.109E-03
	3.000E-01	5.366E-02	-7.297E-05	5.365E-02	1.502E-03	1.564E-03	1.505E-03	3.046E-03	-1.762E-02	2.982E-03
	1.000E-01	5.367E-02	-1.866E-04	5.364E-02	1.501E-03	7.883E-04	1.503E-03	3.022E-03	7.290E-03	3.073E-03
960	9.900E-01	1.701E-02			4.743E-04			9.065E-04		
	9.500E-01	1.702E-02	-8.550E-03	1.701E-02	4.752E-04	-4.903E-02	4.740E-04	4.062E-03	-3.637E+01	6.289E-04
	9.000E-01	1.702E-02	-6.520E-03	1.701E-02	4.745E-04	3.038E-02	4.760E-04	9.250E-04	2.737E+01	1.654E-02
	7.000E-01	1.705E-02	-5.139E-03	1.701E-02	4.748E-04	-2.599E-03	4.743E-04	9.009E-04	1.051E-01	9.353E-04
	5.000E-01	1.707E-02	-3.485E-03	1.702E-02	4.749E-04	-8.137E-04	4.746E-04	9.036E-04	-9.125E-03	8.979E-04
	3.000E-01	1.708E-02	-1.376E-03	1.705E-02	4.749E-04	-1.237E-04	4.748E-04	8.995E-04	8.990E-03	9.093E-04
	1.000E-01	1.709E-02	-8.524E-04	1.706E-02	4.751E-04	-3.641E-04	4.747E-04	9.048E-04	-5.358E-03	8.937E-04

Figure 27 shows the $L_{1,abs}$ norms and the residuals of fitting equation (12) to the $L_{1,abs}$ norms of the density,

temperature, pressure, and material speed when both the time-step controller and spatial resolution are varied. The plus signs indicate the spatial and temporal points (the data points) where the $L_{1,abs}$ norm was computed. The images on the left show the $L_{1,abs}$ norm (the data) while the images on the right show the relative residual of fitting the $L_{1,abs}$ norm to the error model (equation 12). If the residuals of the non-linear least squares fitting procedure are small, then the derived convergence rates are probably reliable. Table 18 details the derived spacetime convergence rates. The fitted rates are generally consistent with values derived when the space and time analyses were performed independently. This result may be due to our choice of fixing the time-step control value rather than the time-step Δt itself.

Table 18
Spacetime Convergence Rates for the Sedov Problem

Parameter	Density	Pressure	Material Speed
A	0.055424	0.00161101	0.000566999
α	0.464093	0.449199	0.8911
ngrid_norm	480	480	480
B	0.42105	-0.0209813	-2.86464
β	3.32e-05	0.000311	0.000907
cstab_norm	0.90	0.90	0.90
C	-0.444463	0.0202671	2.86587
γ	-7.7e-06	8.06e-05	1.99e-05

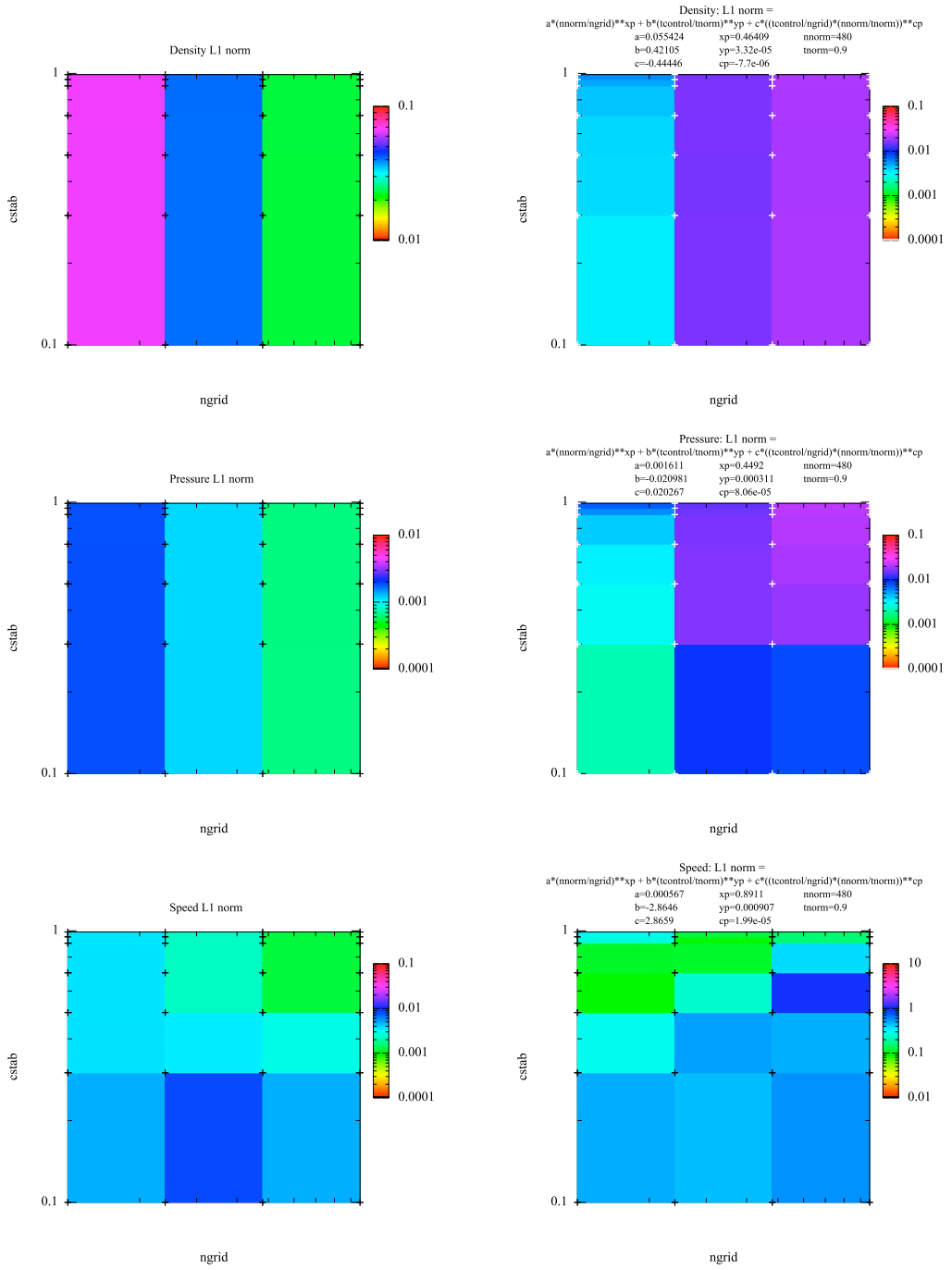

Figure 27. - $L_{1,abs}$ error norms (left) and relative residuals (right) from fitting the error model for the density, pressure, and material speed when spatial and temporal resolution are varied. Plus signs indicate the spacetime points where the error norm was computed.

3. Conclusions and Future Directions

This report has described a spatial-temporal verification analysis on 1D uniform meshes for the Tri-Lab Verification Test Suite. Previous efforts considered only the quantification of spatial discretization errors at fixed values of the time-step controller (Timmes, Gisler & Hrbek 2005). In general, RAGE shows linear rates of convergence in the temporal domain on the Tri-Lab Verification Test Suite. This is consistent with RAGE's first-order accurate time integration procedure, and comparable to what similar codes (e.g., FLASH or ENZO) produce for some of these test problems (Sedov, Noh). For the RMTV, Noh, and Sedov problems the global error norm does not decrease as the temporal resolution is increased because of large persistent errors at discontinuities and boundaries. The error budget for each test problem tends to be dominated by either spatial discretization or temporal discretization errors. We found no cases with significant spatial-temporal cross terms.

The efforts that led to this report spawned a new project to perform a daily execution of an automated spatial-temporal verification analysis for 1D versions of the Tri-Lab Verification Test Suite. Generating numerical solutions, comparing the numerical and analytical solutions, performing the spatial-temporal verification analysis, and plotting the key results has become part of Code Project A's nightly regression testing. In addition to being incorporated into the daily regression tests, all the analytic solution codes, input decks, and `gold' results are now archived on SourceForge.

During the coarse of these investigations a new initialization module for the Reinicke Meyer-ter-Vehn problem was developed in tandem with Mike Clover (SAIC). The new module drastically reduces the size of a RAGE input deck while providing a more accurate and smoother initial state. In addition, Livermore's efforts to deploy the Tri-Lab Verification Test Suite on their codes include the use of four of our analytic solution codes (Su & Olson, Cog8, RMTV, and Mader).

New test problems that exercise multi-material and/or multi-temperature solutions in an extension of the Tri-Lab Verification Test Suite are needed and will be discussed with Livermore and Sandia at NECDC|06. In parallel, calculation verification procedures for complex physics problems that admit no exact solution must be encouraged to advance. The standard approach to conducting verification analysis where no exact solution exists presents two significant limitations. First, computational solutions that converge by oscillation are not calculable, and second, the technique is limited to a simple error model. An improvement to the current method is needed. Calculation verification offers a rigorous procedure for complex physics problems that don't admit an exact solution (Smitherman, Kamm & Brock 2005; Tippett, Kamm, & Timmes 2006). In calculation verification, the absolute value of the pointwise error is calculated, allowing for local oscillatory convergence. The equations are then solved using Newton's method for the convergence constants, discretization errors, and an estimated exact solution simultaneously. This procedure allows for a more complex error model if desired.

Automated verification analysis for 2D and 3D versions of all the existing Tri-Lab test problems are discussed in a companion report (Timmes, Fryxell & Hrbek 2006) which assesses how well RAGE retains fidelity to the underlying physics when motions and gradients are not grid-aligned. As new test problems are added to the Tri-Lab Test Suite, conducting the verification analysis on multi-dimensional versions of the test problems must be encouraged.

Questions of analytic test problem relevance to realistic applications can be addressed by (1) creating new metrics from the existing Tri-Lab Test Suite, (2) constructing new test problems that exercise multi-material and/or

multi-temperature solutions, (3) developing calculation verification into a robust tool capable of performing well on complicated, multi-physics problems, and (4) integrating analyses of the numerical errors from spatial and temporal discretization into quantification of margins and uncertainty (QMU) studies.

4. Acknowledgments

This work was supported by Jerry Brock, Kim New, and Joyce Guzik. The reasoned technical input of Jim Kamm, Chris Fryer, Kunnegunda Belle, Trevor Tippetts, Greg Hutchens, Francois Hemez, Mike Gittings, Mike Clover, and Bill Rider was essential in working through the details of this investigation.

Los Alamos National Laboratory is operated by the Los Alamos National Security, LLC for the National Nuclear Security Administration of the U.S. Department of Energy under contract DE-AC52-06NA25396.

5. References

Brock, J., Isolating Temporal-Discretization Errors for Separate-Verification Analysis, AIAA Aerospace Sciences Conference, January 2004, AIAA-2004-0741, LA-UR-03-9160.

Buchler, J.R., Kollath, Z., & Marom, A., ``An Adaptive Code for Radial Stellar Model Pulsations" , Astrophys. Space Sci. 253, 139, 1997.

Clover, M., Kamm, J.R., & Rider, W.J., ``An Example of Verification Analysis for an Eulerian Hydrocode", LA-UR-00-5371.

Clover, M., Analytic Test Problem Setups in Crestone, in preparation, 2006.

Coggeshall, S.V., Phys. Fluids A, 3, 5, 1991.

Fickett, W., and Davis, W.C., Detonation, (UC Berkeley, 1979).

Fryxell, B., Olson, K.,Ricker, P., Timmes, F.X., Zingale, M., Lamb, D.A., MacNeice, P., Rosner, R., Truran, J.W., & Tufo, K., ``FLASH: An Adaptive Mesh Hydrodynamics Code for Modeling Astrophysical Thermonuclear Flashes", Astrophys. J. Suppl. 131, 273, 2000.

Grove, J., AMHCTOOLS, LA-CC-05-052, 2005a.

Grove, J., AMHCTOOLS, LA-UR-05-7425, 2005b.

Hemez, F.M., ``Non-linear Error Ansatz Models for Solution Verification in Computational Physics" LA-UR-05-8228, 2005.

Kamm, J.R., ``Investigation of the Reinicke & Meyer-ter-Vehn Equations: I. The Strong Conduction Case", LA-UR-00-4304, 2000a.

Kamm, J.R., ``Evaluation of the Sedov-von Neumann-Taylor Blast Wave Solution", LA-UR-00-6055, 2000b.

Kamm, J.R., Rider, W.J., Brock, J.S., ``Consistent Metrics For Code Verification" LA-UR-02-6055, 2002.

Kamm, J.R., and Kirkpatrick, R., Verification analyses of code project A, LA-CP 04-04361, 2004.

Mader, C., Numerical Modeling of Explosives and Propellants, Second Edition CRC Press, Florida, 1997.

Noh, W.F., ``Errors for calculations of strong shocks using an artificial viscosity and an artificial heat flux", J. Comput. Phys. 72, 78-120, 1987.

Reile, C., & Gehren, T., ``Numerical simulation of photospheric convection in solar-type stars I. Hydrodynamical test calculations", Astron. Astrophys. 242, 142, 1991.

Reinicke, P., Meyer-ter-Vehn, J., ``The point explosion with heat conduction", Phys. Fluids A, 1807, 3, 1991

Rider, W.J., ``Revisting Wall Heating", J. Comp. Phys., 162, 395, 2000.

Smitherman, D.P., Kamm, J.R., Brock, J.S., ``Calculation Verification: Pointwise Estimation of Solutions and Their Method-associated Numerical Error", LA-UR-05-8002, 2005.

Swesty, F.D., & Myra, E.S., ``A Numerical Algorithm for Modeling Multigroup Neutrino-Radiation Hydrodynamics in Two Spatial Dimensions", Astrophys. J., submitted, 2006.

Su, B., and Olson, G.L., J. Quant. Spectro. Radiat. Transfer, 56, 3, 1996.

Taylor, G.I., ``The formation of a blast wave by a very intense explosion", Proc. Roy. Soc. London A 201, 159, 1950).

Timmes, F.X., Clover, M., On a Cell-Averaged Solution to the Coggeshall #8 Problem, in preparation, 2006.

Timmes, F.X., Gisler, G., Hrbek, G.M., Automated Analyses of the Tri-Lab Verification Test Suite on Uniform and Adaptive Grids for Code Project A, LA-UR-05-6865, 2005.

Timmes, F.X., Fryxell, B., Hrbek, G.M., ``Two- and Three-dimensional properties of the Tri-Lab Verification Test Suite for Code Project A", LA-UR-06-6697, 2006.

Tippett, T, Timmes, F.X., & Kamm, R.J., Calculation Verification for Code Project A, in preparation, 2006.

Williams, T., et al., gnuplot 4.0 Users Manual, 2004.

6. Appendix A - Input Decks

6.1 For the Su & Olson Problem

```
pname = ``suo_100pt" ! problem name

! MESH SETUP
! 25 cm thick 1-D slab
! recommendation: Do not use the mesh variables numrho, numfine, numlev,
! smallke, and mxcells. Rather use sizemat.

imxset = 100
dxset = 0.25

! CALCULATION CONTROL
tmax = 1.0e-9 ! Ending simulation time in sec
dtedt(1) = 1.0e-9 ! dumpts at exactly these times
dodmpxdt = .true. ! turns on dt adjustment to get dumps at exact dedt time
tedit = 1.0e-9 ! time frequency of binary dump files

kread = -1 ! kread < 0 is new problem; kread>=0 = restart cycle
uselast = .true. ! if .true. and kread<0, ``pname-lastdump" = restart file
ncmax = 400000 ! Max # of cycles
dtnext = 1.0e-16 ! initial time step
dtmax = 7.5e-12 ! maximum dt allowed = 0.9d0*(min dx)/clight
dtpct = 0.1 ! adjusts init. time step only
de_tevpct = 0.01 ! percentage max change in tev from radiation
de_tevmin = 12.5 ! tev floor, below which de_tevpct is ignored
siepct = 0.2 ! percentage max change in specific internal energy
tevcut = 12.5 ! tev floor, below which siepct is ignored

ncedit = 0 ! disable cycle frequency for binary dumps
modcyc = 10000 ! frequency of status edits
shortmodcyc = 20 ! frequency of short edits
ndtedt = 0 ! number of simulation times for std edits (default=0)

! PHYSICS MODULES
dohydro = .false. ! turn off hydro for this Marshak problem (default=.true.)
doheat = .false. ! turn off heat conduction
dorad = .true. ! turn on radiation

! RADIATION
onetemp = .false. ! 2-T non-equilibrium diffusion
fluxlim = .false. ! switch for radiation fluxlimiter

! MATERIALS
nummat = 1 ! number of materials

! Use sizemat to control mesh refinement. Note that this has to be
! coordinated with the dxset parameter above.

sizemat(1) = 0.25 ! 1 level of refinement for material 1
!sizemat(1) = 0.125 ! 2 levels, effective 200 points
!sizemat(1) = 0.0625 ! 3 levels, effective 400 points
!sizemat(1) = 0.03125 ! 4 levels, effective 800 points
!sizemat(1) = 0.015625 ! 5 levels, effective 1600 points
!sizemat(1) = 0.0078125 ! 6 levels, effective 3200 points
!sizemat(1) = 0.00390625 ! 7 levels, effective 6400 points

! EOS and OPACITY
```

```
keos = -3 ! 0 = ideal gas; 1 = sesame; 2 = N/A; 3 = new TEOS files;
! keos < 0 for special analytic EOS
! for the su-olson problem, use keos = -3 for e = aT**4

matdef(1,1) = 0.0 !
matdef(61,1) = 0 ! power law opacity: kappa = coef*(tev/tevz)**power
matdef(62,1) = 1. ! krmax
matdef(63,1) = 0.0 ! power
matdef(64,1) = 1.0 ! coef
matdef(65,1) = 1.0 ! tevz
matdef(66,1) = 1.0e-20 ! krscat, 0.201 for Thompson scattering, krtot = krscat + kra
!
! REGIONS
numreg = 1
matreg(1) = 1
rhoreg(1) = 1.0 ! density gm/cc
tevreg(1) = 1.0e-1 ! T eV

! CONSTANT FLUX BC
nomilne = .false. ! default = .false.
milne_option = 1 ! sets milne BC to true milne (0=Dirchlett, 2=Spillman)
tevbcl = 1000. ! Trad = 1 keV
```

6.2 For the Coggeshall #8 Problem

```
pname = ``cog_100pt''
test_pname = ``r008_3v''

! CONTROL
time = 1.0e-8 ! starting time; super important for proper initialization
tmax = 2.0e-8 ! Ending simulation time in sec
dtedt(1) = 2.0e-8
dodmpxdt = .true. ! turns on dt adjustment to get dumps at exact dedt time
tedit = 2.0e-8 ! time frequency of binary dump files
dtnext = 1.0e-16 ! initial time step
dtmax = 1.0 ! maximum dt allowed
!dtforce = 1.0e-9
tstab = 0.20 ! max timestep based on material velocity

kread = -1
uselast = .true.
ncmax = 400000
ncedit = 0
modcyc = 0
shortmodcyc = 20

dohydro = .true.
dorad = .false.
doheat = .true.

! GRID
! RECOMMENDATION: Do not use the mesh variables numrho, numfine, numlev,
! smallke, and mxcells. Rather use sizemat.

imxset = 100
dxset = 0.02
```

```
cylin = .false.
sphere = .true.


! MATERIALS
keos = 0
nummat = 1

! Use sizemat to control mesh refinement.  Note that this has to be
! coordinated with the dxset parameter above.

sizemat(1) = 0.02 !  1 level of refinement for material 1
!sizemat(1) = 0.01 !  2 levels, effective 200 points
!sizemat(1) = 0.005 !  3 levels, effective 400 points
!sizemat(1) = 0.0025 !  4 levels, effective 800 points
!sizemat(1) = 0.00125 !  5 levels, effective 1600 points
!sizemat(1) = 0.000625 !  6 levels, effective 3200 points
!sizemat(1) = 0.0003125 !  7 levels, effective 6400 points

matdef(1,1) = 0.0
matdef(16,1) = 0.6666666666
matdef(30,1) = 1.0e12 !  specific heat 1.e12 erg/g/ev = 0.1 jk/g/kev

! Opacity

matdef(61,1) = 0 !  Analytic Opacity:
matdef(62,1) = 1.0e20 !  krmax
matdef(63,1) = +2.0 !  Power:  (tevz/te)**powt
matdef(64,1) = 5.485 !  Coef:  4*arad*tevz**3/3/coef = thermcoeff
matdef(65,1) = 1000.0 !  tevz
matdef(66,1) = 0.0 !  krscat
matdef(67,1) = 1.000 !  kpscale
matdef(68,1) = 0.000 !  rho**powd

! Thermal Conductivity
matdef(81,1) = 0
matdef(82,1) = 1.e21 !  Thermcoef 1.e21 erg/ev/cm/s = 1.0 jk/kev/cm/sh
matdef(83,1) = 5.0 !  powt:  (te/tevz)**powt
matdef(84,1) = 1000.  !  tevz
matdef(85,1) = -1.0 !  powd:  rho**powd

! REGIONS

numreg = 2

matreg(1) = 1
rhoreg(1) = 1.0
siereg(1) = 1.0e12

matreg(2) = 1
rhoreg(2) = 3.0
tevreg(2) = 100.0
xdreg(2) = 1.0
xlreg(2) = 0.
xrreg(2) = 2.0

freeze_num = 1
freeze_x_lo(1) = 1.98
freeze_x_hi(1) = 2.00
```

6.3 For the Mader Problem

```
pname = ``mad_100pt"

! grid
! do not use the mesh variables numrho, numfine, numlev,
! smallke, and mxcells.  rather use sizemat.

imxset = 102
dxset = 0.05
norecon = .true.  ! supress all amr

!CONTROL
tmax = 5.00e-6 !  Ending simulation time in sec
dtedt(1) = 5.00e-6 !  dumps at these exact times
dodmpxdt = .true.  !  turns on dt adjustment to get dumps at exact dedt time
tedit = 5.00e-6 !  time frequency of binary dump files
dtnext = 1.0e-16 !  initial time step
dtmax = 1.0e-5 !  maximum dt allowed

kread = -1 !  kread < 0 is new problem; kread>=0 = restart cycle
uselast = .true.  !  if .true.  and kread<0, ``pname-lastdump" = restart file
ncmax = 500000 !  Max # of cycles
ncedit = 0 !  disable cycle frequency for binary dumps
modcyc = 0 !  frequency of status edits
shortmodcyc = 20 !  frequency of short edits

mincellpe = 0 !  minimum number of cells per processor
maxcellpe = 0 !  minimum number of cells per processor
secdump = 3600.0 !  wall clock seconds between even & odd dumps

! MATERIALS
eosfile = 'val.teos'
keos = 3
nummat = 4
matdef(1,1) = 5030 !  sesame air
matdef(1,2) = 3719 !  sesame Al
matdef(1,3) = 152777 !  Hom solid
matdef(1,4) = 162777 !  GAMMA LAW Validation HE

! Use sizemat to control mesh refinement.  Note that this has to be
! coordinated with the dxset parameter above.

sizemat(1) = 0.05 !  1 levels, effective 100 points
sizemat(2) = 0.05 !
sizemat(3) = 0.05 !
sizemat(4) = 0.05 !

!sizemat(1) = 0.025 !  2 levels, effective 200 points
!sizemat(2) = 0.025 !
!sizemat(3) = 0.025 !
!sizemat(4) = 0.025 !

!sizemat(1) = 0.0125 !  3 levels, effective 400 points
!sizemat(2) = 0.0125 !
!sizemat(3) = 0.0125 !
!sizemat(4) = 0.0125 !

!sizemat(1) = 0.00625 !  4 levels, effective 800 points
!sizemat(2) = 0.00625 !
!sizemat(3) = 0.00625 !
```

```
!sizemat(4) = 0.00625 !

!sizemat(1) = 0.003125 ! 5 levels, effective 1600 points
!sizemat(2) = 0.003125 !
!sizemat(3) = 0.003125 !
!sizemat(4) = 0.003125 !

!sizemat(1) = 0.0015625 ! 6 levels, effective 3200 points
!sizemat(2) = 0.0015625 !
!sizemat(3) = 0.0015625 !
!sizemat(4) = 0.0015625 !

! REGIONS

numreg = 3

matreg(1) = 1 ! air
prsreg(1) = 1.0e6
tevreg(1) = 0.025

matreg(2) = 3 ! solid VHE
xlreg(2) = 0.0000
xrreg(2) = 5.00000
prsreg(2) = 1.0e6
tevreg(2) = 0.025

! already burned material, keep as thin as possible
! to minimize artifacts of a ``thick ignitor''
matreg(3) = 4
xlreg(3) = 5.00000
xrreg(3) = 5.1000
rhoreg(3) = 2.500
tevreg(3) = 0.2

! HE setup
!he_size = -5.0 ! appears to be a dead parameter
he_dtpct = 0.5 ! time step controller dt = (dx/v_det) * he_dtpct
he_number = 1 ! number of explosive pairs
he_unreacted(1) = 3 ! region 3
he_reacted(1) = 4 ! region 4
he_rate_size(1) = 0.40 ! used to make rate cell size independent
he_model(1) = 2 ! Forest Fire
he_energy(1) = 0.0 ! reaction energy
he_pcrush(1) = 10.0e9 ! Multiple Shock Forest Fire
he_detvel(1) = 8.000e5 ! denonation speed
he_rhoz(1) = 1.875 ! unreacted initial density
he_pmin(1) = 10.0e9 ! Minimum Forest Fire Pressure
he_pcj(1) = 300.0e9 ! cj pressure
he_num_coef(1) = 7 ! number of explosive constants
he_constants(1,1) = -7.4335806250e05,
7.5179600000E+05,-3.0147946875E+05,6.15952500000E+04,
-6.89248339844E+03,4.5775354003E+02,-1.80467948914E+01
```

6.4 For the Reinicke & Meyer-ter-Vehn Problem

```
pname = ``rmtv-100pt''
test_pname = ``r006_3v02''
```

```
! set the parameters of the trilab rmtv problem
userparms(1) = 234.209e16 ! energy in egs
userparms(2) = 4.0e13 ! (gamma - 1) * cv in erg/k
userparms(3) = 0.25 ! gamma - 1


! time step controllers
tmax = 0.051251245293611e-8
dtedt(1) = 0.051251245293611e-8
dodmpxdt = .true. ! turns on dt adjustment to get dumps at exact dedt time
tedit = 0.051251245293611e-8
dtnext = 1.0e-20 ! initial time step
dtmax = 1.0 ! maximum dt allowed
!dtforce = 1.0e-12
siepct = 0.2 ! percentage max change in specific internal energy
tevcut = 1.0e-6 ! tev floor, below which siepct is ignored

! cycle controllers
kread = -1
uselast = .true.
ncmax = 500000
ncedit = 0 ! disable cycle frequency for binary dumps
modcyc = 0 ! frequency of status edits
shortmodcyc = 100 ! frequency of short edits
mincellpe = 0
maxcellpe = 0

! hydro and heat conduction only
dohydro = .true.
doheat = .true.
dorad = .false.
onetemp = .true.
fluxlim = .false.

! GRID
! RECOMMENDATION: Do not use the mesh variables numrho, numfine, numlev,
! smallke, and mxcells. Rather use sizemat.

imxset = 100
dxset = 0.01
norecon = .true. ! supress all amr

cylin = .false.
sphere = .true. ! Sphere only in 1-D calculations:

! MATERIALS
nummat = 2 ! must have two material for cog8

! Use sizemat to control mesh refinement. Note that this has to be
! coordinated with the dxset parameter above.

sizemat(1) = 0.01 ! 1 level of refinement for material 1
!sizemat(1) = 0.005 ! 2 levels, effective 200 points
!sizemat(1) = 0.0025 ! 3 levels, effective 400 points
!sizemat(1) = 0.00125 ! 4 levels, effective 800 points
!sizemat(1) = 0.000625 ! 5 levels, effective 1600 points
!sizemat(1) = 0.0003125 ! 6 levels, effective 3200 points

sizemat(2) = 0.01 ! 1 level of refinement for material 1
!sizemat(2) = 0.005 ! 2 levels, effective 200 points
```

```
!sizemat(2) = 0.0025 !  3 levels, effective 400 points
!sizemat(2) = 0.00125 !  4 levels, effective 800 points
!sizemat(2) = 0.000625 !  5 levels, effective 1600 points
!sizemat(2) = 0.0003125 !  6 levels, effective 3200 points

! EOS
keos = 0
matdef(16,1) = 0.25 !  gamma-1 ==> gamma = 5/4
matdef(30,1) = 4.0e13 !  Cv 1.e13 ==> 1 jk/kev/g

matdef(16,2) = 0.25 !  gamma-1 ==> gamma = 5/4
matdef(30,2) = 4.0e13 !  Cv 1.e13 ==> 1 jk/kev/g

! Opacity
! The analytic models are structured such that Rosseland mean
! absorption coefficient (units:  cm**2/g) for this material,
! integrated over all frequencies, is equal to
!
! coef * (tevz/tev_use)**powt * (frac_mass/frac_vol)**powd
! with
! kramax = matdef(62,m) !  recommended default = 1.0e30
! powt = matdef(63,m) !  recommended default = 3
! coef = matdef(64,m) !  recommended default = 0.0
! tevz = matdef(65,m) !  recommended default = 1000.0
! krscat = matdef(66,m) !  recommended default = 0.2
! kpscale = matdef(67,m)
! powd = matdef(68,m) !  recommended default = 0
! model = matdef(69,m) !  recommended default = 1
! hnu_edge = matdef(70,m) !  recommended default = 0.0
! pct_jump = matdef(71,m) !  recommended default = 0.0

matdef(61,1) = 0 !  use analytic opacity
matdef(62,1) = 1.0e10 !  krmax:
matdef(63,1) = +3.5 !  power-in-temp-dependence:  ``powt'' in (tevz/te)**powt
matdef(64,1) = 5.48806 !  overall coefficient ``coef''
matdef(65,1) = 1000.0 !  reference temperature ``tevz''
matdef(66,1) = 0.001 !  ?scattering factor?  ``krscat''
matdef(67,1) = 1.000 !  kpscale:  opacity multiplier
matdef(68,1) = 1.000 !  power-in-density-dependence:  ``powd'' in (frac_rho)**powd

matdef(61,2) = 0 !  use analytic opacity
matdef(62,2) = 1.0e10 !  krmax:
matdef(63,2) = +3.5 !  power-in-temp-dependence:  ``powt'' in (tevz/te)**powt
matdef(64,2) = 5.48806 !  overall coefficient ``coef''
matdef(65,2) = 1000.0 !  reference temperature ``tevz''
matdef(66,2) = 0.001 !  ?scattering factor?  ``krscat''
matdef(67,2) = 1.000 !  kpscale:  opacity multiplier
matdef(68,2) = 1.000 !  power-in-density-dependence:  ``powd'' in (frac_rho)**powd

! Thermal Conductivity
! The analytic thermal conductivity model uses the following
! formula for the thermal conductivity:
!
! thermcoef * rho**powd * (te/tevz)**powt
! with
! thermcoef = matdef(82,nm)
! powt = matdef(83,nm)
! tevz = matdef(84,nm)
! powd = matdef(85,nm)

matdef(81,1) = 0 !  use thermal conductivity
```

```
matdef(82,1) = 1.e21 ! thermcoef 1.e21 erg/ev/cm/s = 1.0 jk/kev/cm/sh
matdef(83,1) = 6.5 ! power-in-temp-dependence: ``powt'' in (te/tevz)**powt
matdef(84,1) = 1000.0 ! reference temperature: ``tevz''
matdef(85,1) = -2.0 ! power-in-density-dependence: ``powd'' in rho**powd

matdef(81,2) = 0 ! use thermal conductivity
matdef(82,2) = 1.e21 ! thermcoef 1.e21 erg/ev/cm/s = 1.0 jk/kev/cm/sh
matdef(83,2) = 6.5 ! power-in-temp-dependence: ``powt'' in (te/tevz)**powt
matdef(84,2) = 1000.0 ! reference temperature: ``tevz''
matdef(85,2) = -2.0 ! power-in-density-dependence: ``powd'' in rho**powd

! REGIONS
numreg = 1
matreg(1) = 1
rhoreg(1) = 1.0 ! test_pname will set these...
tevreg(1) = 0.01
```

6.5 For the Noh Problem

```
pname = ``noh-100pt'' !Problem name

! CONTROL
tmax = 0.3 !Maximum simulation time (real time in sec.)
dtedt(1) = 0.3
dodmpxdt = .true. ! turns on dt adjustment to get dumps at exact dedt time
tedit = 0.3 !Frequency of edit dumps in real simulation time
dtnext = 1.0e-16 ! initial time step
!dtforce = 1.0e-12
tstab = 0.2

kread = -1 ! kread<0 is new problem; kread>=0 then restart cycle = kread
uselast = .true. ! If true and kread<0 then use ``pname-lastdump'' as restart file
ncmax = 500000 ! Maximim # of cycles
ncedit = 0 ! Frequency of edit dumps in # of cycles
modcyc = 0 ! Frequency of status edits in # of cycles
shortmodcyc = 10 ! Frequency of short edit dumps
mincellpe = 0 ! don't enforce minimum cell count per processor
maxcellpe = 0 ! don't enforce maximum cell count per processor

! GRID
! RECOMMENDATION: Do not use the mesh variables numrho, numfine, numlev,
! smallke, and mxcells. Rather use sizemat.

imxset = 100 !Number of level 1 cells in the x-direction
dxset = 0.01 !Size of level 1 cells in x-direction
!numfine = 16

cylin = .false. !true=r-z cylindrical geometry; false=not cylindrical
sphere = .true. !true=spherical geometry; false=not spherical

dohydro = .true. ! hydrodynamics problem
doheat = .false. ! no heat conduction
dorad = .false. ! no radiation

! MATERIALS

nummat = 1 !Number of materials
```

```
! Use sizemat to control mesh refinement.  Note that this has to be
! coordinated with the dxset parameter above.

sizemat(1) = 0.01 !  1 level of refinement for material 1
!sizemat(1) = 0.005 !  2 levels, effective 200 points
!sizemat(1) = 0.0025 !  3 levels, effective 400 points
!sizemat(1) = 0.00125 !  4 levels, effective 800 points
!sizemat(1) = 0.000625 !  5 levels, effective 1600 points
!sizemat(1) = 0.0003125 !  6 levels, effective 3200 points

! EOS
keos = 0 !0 = ideal gas EOS; 1 = SESAME EOS; 2 = N/A; 3= new TEOS files
matdef(16,1) = 0.6666667 !Specifying (gamma-1) Gamma = 5/3
matdef(30,1) = 1.0e12 !Specifying Cv - specific heat [erg/gm/ev]

! REGIONS
numreg = 1 !Number of regions

matreg(1) = 1 !Region 1 is of material 1
rhoreg(1) = 1.0 !Density of region 1 [gm/cc]
siereg(1) = 1.0e-10 !Specific Internal energy of region 1 [erg/gm]
xdreg(1) = -1.0 !Initial radial velocity of region 1 [cm/s]

! ``freeze regions'' are inflow/outflow boundary conditions for an Eulerian mesh
! freeze_x_lo and freeze_x_hi determine the extent of the freeze region in
! the x-direction [cm].  The region goes from freeze_x_lo to freeze_x_hi.

freeze_num = 1 !Number of freeze regions
freeze_x_lo(1) = 0.90 !  Begin freeze region in x-direction [cm]
freeze_x_hi(1) = 1.00 !  End of freeze region in x-direction [cm]
```

6.6 For the Sedov Problem

```
pname = ``sed-120pt'' !Problem name

! CONTROL
tmax = 1.0 !Maximum simulation time (real time in seconds)
dtedt(1) = 1.0
dodmpxdt = .true.  !  turns on dt adjustment to get dumps at exact dedt time
tedit = 1.0 !Frequency of edit dumps in real simulation time
dtnext = 1.0e-16 !  initial time step
!dtforce = 1.0e-12
cstab = 0.9 !  courant timestep controller

kread = -1 !kread<0 is a new problem; kread>=0 then restart cycle=kread
uselast = .true.  !If true and kread<0 then use ``pname-lastdum'' as restart file
ncmax = 500000 !Maximum # of cycles
ncedit = 0 !  disable cycle frequency for binary dumps
modcyc = 0 !  frequency of status edits
shortmodcyc = 200 !  frequency of short edits

dohydro = .true.  !true=hydro routines turned on (default); false=hydro not on
doheat = .false.  !true=do heat conduction; false=do not do heat cond.(default)
onetemp = .true.  !true=equil.  diffusion (one temperature)
!false=nonequilibrium diffusion (two temperatures) (default)

! GRID
```

```
! RECOMMENDATION: Do not use the mesh variables numrho, numfine, numlev,
! smallke, and mxcells.  Rather use sizemat.

imxset = 120 !Number of Level 1 zones in the x-direction:
dxset = 0.01 !Size of Level-1 zones in the x-direction:
norecon = .true.  !  supress all amr

cylin = .false.  !true=r-z cylindrical geometry; false=not cylindrical
sphere = .true.  !true=spherical geometry; false=not spherical


! MATERIALS
nummat = 1 !Number of materials

! Use sizemat to control mesh refinement.  Note that this has to be
! coordinated with the dxset parameter above.

sizemat(1) = 0.01 !  1 level of refinement for material 1
!sizemat(1) = 0.005 !  2 levels, effective 240 points
!sizemat(1) = 0.0025 !  3 levels, effective 480 points
!sizemat(1) = 0.00125 !  4 levels, effective 960 points
!sizemat(1) = 0.000625 !  5 levels, effective 1920 points
!sizemat(1) = 0.0003125 !  6 levels, effective 3840 points

! EOS
keos = 0 !Use ideal gas equation of state
matdef(16,1) = 0.4 !Specifying (gamma-1); gamma = 1.4
matdef(30,1) = 1.0e-4 !Specifying Cv - specific heat [erg/gm/ev]


! REGIONS
numreg = 2 !Number of regions

matreg(1) = 1 !Region 1 is of material 1
rhoreg(1) = 1.0 !Density of region 1 [gm/cc]
siereg(1) = 2.539731e-8 !Specific internal energy of region 1 [erg/g]

matreg(2) = 1 !Region 2 is of material 1
rhoreg(2) = 1.0 !Density of region 2 [gm/cc]
siereg(2) = 2.539731e+4 !Specific internal energy of region 2 [erg/g]
xlreg(2) = 0.0 !Left x-boundary of region 2
xrreg(2) = 0.02 !Right x-boundary of region 2
```